Water Air Soil Pollut (2024) 235:319
https://doi.org/10.1007/s11270-024-07125-1

Urban Development and Climate Change: Implications for Educational Tourism Destination Planning

Hamed Rezapouraghdam ·
David Hidalgo-García

Received: 23 November 2023 / Accepted: 2 May 2024 / Published online: 9 May 2024

Abstract Global warming caused by greenhouse gas emissions, transportation, and the transformation of land use caused by population growth is a critical problem that requires immediate and urgent interventions, especially in popular tourism destinations where the impact on quality of life is intense. In recent years, while new urban developments have been carried out for higher education institutions, less attention has been paid to the environmental implications of such expansions. Surprisingly, despite a growing interest in climate change action in educational institutions, little is known about the link between Land Surface Temperature (LST) variability and Surface Urban Heat Island (SUHI) of university campuses and their host communities. To fill the gaps mentioned earlier, this study aims to provide a comprehensive analysis of the spatial and temporal variability of the SUHI and the LST within a university campus and its surrounding urban environment. Using Sentinel 3 images and the TsHARP algorithm, the LST was determined, the SUHI was calculated, and the hot spots were obtained in an educational tourism hub; Famagusta, Cyprus. The Panel Data and ANOVA techniques were used for the subsequent analysis of the findings. Findings indicated that due to its low-rise buildings and large green areas, the studied campus not only had little contribution to the creation of SUHI but even minimized its effects on the urban areas attached to it. These findings provide valuable implications for authorities in standardizing criteria for future university establishments.

Keywords Surface Urban Heat Island (SUHI) · Land Surface Temperature (LST) · Land use changes · Remote sensing · University campus · Community development

1 Introduction

One of the most critical challenges that humanity needs to deal with today is the extreme weather events linked to global warming (An et al., 2020; Santamouris, 2020). The transformation and modification of soil through the increase of new areas motivated by the significant growth of the population is a process that contributes significantly to global warming (Song et al., 2020). The forecast is that by 2050 the urban population will reach 70% of the total population (UNO, 2018). But these processes not only increase the LST on their own but also generate an increase in greenhouse gas emissions (Blessy et al., 2023) due to the industrial construction and

H. Rezapouraghdam
Faculty of Tourism, Eastern Mediterranean University, TRNC, Via Mersin 10, Gazimagusa 99628, Turkey
e-mail: hamed.rezapouraghdam@emu.edu.tr

D. Hidalgo-García (✉)
Technical Superior School of Building Engineering, University of Granada, Granada, Spain
e-mail: dhidalgo@ugr.es

manufacturing process. The forecasts for the years 2041–2060 are not positive and continue to report an increase of around 23.8% in environmental emissions (Zhang et al., 2021). In turn, CO_2 from construction materials that are usually used in urban areas causes a process called carbonization (Zhao et al., 2023) that further increases the concentrations of this gas in the atmosphere.

The greatest increases in LST are occurring in urban areas where the urban climate alteration phenomenon called Urban Heat Island (UHI) is prevalent. Some studies (Santamouris, 2020) report that this phenomenon is intensified by human activities. In this way, and usually, temperatures in rural areas are lower than in urban areas. This circumstance produces a degradation of air quality, loss of biodiversity (Arnfield, 2003), and an increase in morbidity (Arbuthnott & Hajat, 2017), which worsens people's quality of life (Macintyre et al., 2018).

In recent decades, remote sensing has allowed the generation of a methodology that allows quick and accurate evaluation of changes in the urban surface and urban climate. The appearance and implementation of thermal sensors have made it possible to investigate issues related to temperatures, such as LST and SUHI (Song et al., 2018). The relationship between the LST and the different land covers (LULC) is very important to establish and determine the importance of how changes in the covers due to the building process can affect the LST and thus the SUHI (Tepanosyan et al., 2021). Recently, a study was carried out in New York City between 2001 and 2020 (Yin et al., 2023) that reported an increase in LST of between 3 and 4ºC, mainly motivated by changes in urban coverage that very negatively affected the environmental comfort of 50% of the population. Along these lines, the study carried out in the city of Granada (Spain) between 1985 and 2020 reported an increase in the LST stemmed mainly from changes in LULC (Hidalgo García and Arco-Díaz, 2022). These changes in LULC and increases in LST affect people's quality of life (Das & Das, 2020). For all these reasons, it is vitally important to analyze extreme temperature changes in urban areas.

One of the thermal comfort indices commonly used to determine thermal well-being is the Thermal Field Variance Index (UTFVI). Urban spaces with high temperatures known as Urban Hot Spot (UHS) (Sharma et al., 2021) are also related to the different LULC coverages. Recent studies have reported that the urban areas with the highest values of LST and SUHI contain the areas identified as UHS and warn of significant growth of these during the last decade (Amindin et al., 2021). Recently, studies were carried out in the cities of Delhi and Mumbai (India) between the years 1991–2018 (Shahfahad et al., 2021) and in the city of Granada (Spain) (Hidalgo García and Arco-Díaz, 2022) between the years 1985 and 2020 reported that the areas classified as UHS were located in the areas with the highest UTFVI index and, therefore, with the areas with the highest LST values.

In recent years motivated by the increase in the number of university students, an important boom has been taking place in the transformation of land uses for the construction of university campuses (Cheng et al., 2020). Therefore, the development of university campuses should be considered an important element in the study of the SUHI of adjoining urban areas due to the ability of these large surfaces to alter the urban climate. In this way and for a few years, the study of the variation of the LST and SUHI on university campuses through remote sensing has begun. For instance, the study of the Wangling campus of Sichuan University (China) reported LST differences of up to 4 K within the campus (Cheng et al., 2020), the study on the campuses of the University of Indonesia and the University of Malaya (Malaysia) between 2013 and 2016 reported differences in SUHI of up to 8 K between the different areas of the campus (Wibowo et al., 2020). The study carried out between 2014 and 2019 on the campus of King Abdelaziz University in Jeddah (Saudi Arabia) reported LST differences between different areas of the campus of between 7 and 9 K. In turn, negative correlations were reported between vegetation and LST (Addas et al., 2020).

However, we found a main drawback and that is that the existing literature only studies the relationships of the LST and SUHI in the interior space of the campus, not taking into account its relationship with the city that hosts it. It is important to note that SUHI is a phenomenon of alteration of the urban climate and therefore, it is necessary to study it globally and not locally (Gaur et al., 2018; Keeratikasikorn & Bonafoni, 2018). At the same time, it also happens that these investigations use LST values calculated using Landsat 8 images whose main characteristics are a resolution of 100 m and an orbit constantly every 16 days. Consequently, the LST and SUHI

findings in these studies are representative of the specific day(s) chosen for analysis and coincide with the satellite's overpass time. These studies extrapolated the results obtained to longer periods to obtain global results of LST and SUHI on campus. This is not the correct approach as recent research (Anjos et al., 2020; Hidalgo García and Arco-Díaz, 2022) indicates the existence of significant variability of SUHI and LST, both throughout the day and over time. For this reason, having the availability of daily images derived from satellites that orbit the same place several times a day, such as MODIS or Sentinel 3, is an important element. However, these satellites have a major drawback in that the resolution of thermal images is 1000 m, which is not an adequate pixel size on small campuses. Nevertheless, a multitude of studies and research endeavours employ the TsHARP algorithm, enabling the conversion of these low-resolution images (1000 m) into fresh high-resolution images with a pixel size of 10 m (Belgiu & Stein, 2019; Huryna et al., 2019; Zhou et al., 2020). In this way, by using high-resolution Sentinel 3 images, more precise LST and SUHI results can be achieved in the study of urban areas.

The objective of this research is to study and analyze the spatio-temporal variability of the LST and SUHI using high-resolution Sentinel 3 images over Northern Cyprus. This small island state is usually known as a center of educational tourism as it is home to numerous universities that receive international students from more than 100 countries (Rezapouraghdam et al., 2022a, b). Of all the existing universities in Northern Cyprus, EMU is the only public one and is also the largest and oldest in the region. For this reason, it was selected to be investigated in this study. To this end, the city where the EMU is located was classified using the world-known classification of Local Climatic Zones (LCZ). This will allow us to fully understand the variability of the LST and SUHI of each LCZ and, in turn, be able to extrapolate our results to any other city with similar characteristics. Using Sentinel 2 images, the Proportion Vegetation (PV), LULC, and the normalized difference vegetation index (NDVI) were obtained. By using the TsHARP algorithm and Sentinel 3 images, the LST was obtained and the SUHI and UHS were determined in order to determine the different areas according to the UTFVI classification. Subsequently, and after obtaining all the data, they were statistically analyzed using Panel Data and ANOVA techniques. This statistical analysis methodology can be considered more appropriate.

Concerning existing research, the application of this method presents an innovative element by including high-resolution daytime and nighttime thermal images thanks to the use of the Sentinel 3 sensor and the use of the TsHARP algorithm. This method is different from traditional studies where they use a single image per day using the Landsat satellite. Therefore, our research will allow us to analyze the variability of the variables mentioned at various times of the day and obtain more complete results. In turn, our research not only analyzes the structure of the campus but also the city where it is located through the LCZ classification (Stewart & Oke, 2012). This allows us to have the possibility of understanding and analyzing how the EMU university campus could influence the urban climate of the city where it is hosted. With this research, the authors intend to answer the following questions:

1. How are SUHI and LST developed in the host city and the university campus?
2. Is the urban development of the university important in the variability of the SUHI and LST of the city?
3. Is there any relationship between the indices (PV, LULC, and NDVI) and the areas with higher temperatures?
4. How the findings of this study can contribute to the sustainable urban planning and development of university campuses?

The insights derived from this investigation can play a pivotal role in alleviating the ramifications associated with heightened SUHI, LST, and UHS, thereby enhancing the environmental comfort index in these locales and the adjoining urban regions. Ultimately, this transformation can contribute to the creation of sustainable environments capable of withstanding the challenges posed by global warming.

2 Materials and Methods

2.1 Research area

The area under study (Fig. 1) is the city of Famagusta, where the campus of the Eastern Mediterranean University (EMU) is located.

This location is a popular vacation spot and an educational tourism center that attracts many international students annually (Rezapouraghdam et al., 2022a, b). Accordingly, as an island state, the issues of climate change, sustainable planning, and development are highly critical topics in this travel hub (Rezapouraghdam & Vahedi, 2024). The average annual temperature of this destination ranges from 297.15 K to 306.15 K in January and July, respectively. However, a minimum of 279.15 K can be reached in winter, and a maximum of 310.15 K can be reached in summer. The city has an average of 3,978 h of sunshine per year. The population of Famagusta is 57,442 inhabitants and it has an area of 1,979 km^2, resulting in an average population density of 29.02 inhabitants/km^2. Since 1979, the Eastern Mediterranean University has started to provide higher education, and today it hosts a total of 16,000 students within an area of 0.87 km^2. The campus consists of 15 buildings for faculties, 3 for administrative purposes, and 21 for residential and other uses. These buildings cover 55% of the campus area, while the remaining 45% is allocated to green spaces (Fig. 2).

2.2 Methodology

Figure 3 describes the methodology carried out in this research. Using Sentinel 2 images, the NDVI, PV, and LULC were determined at a resolution of 10 m. The Support Vector Machine (SVM) methodology was implemented for land cover classification within the QGIS software, and the accuracy of the land cover classification was assessed using a precision matrix (Xu et al., 2009). This tool allows a classification to be carried out through an autonomous learning system. Its main objective is to establish and determine a decision-making process to classify and determine the different classes automatically previously established.

Subsequently, NDVI and PV images were extracted from the Ocean and Land Cover Instrument (OLCI) multispectral sensor, providing a spatial

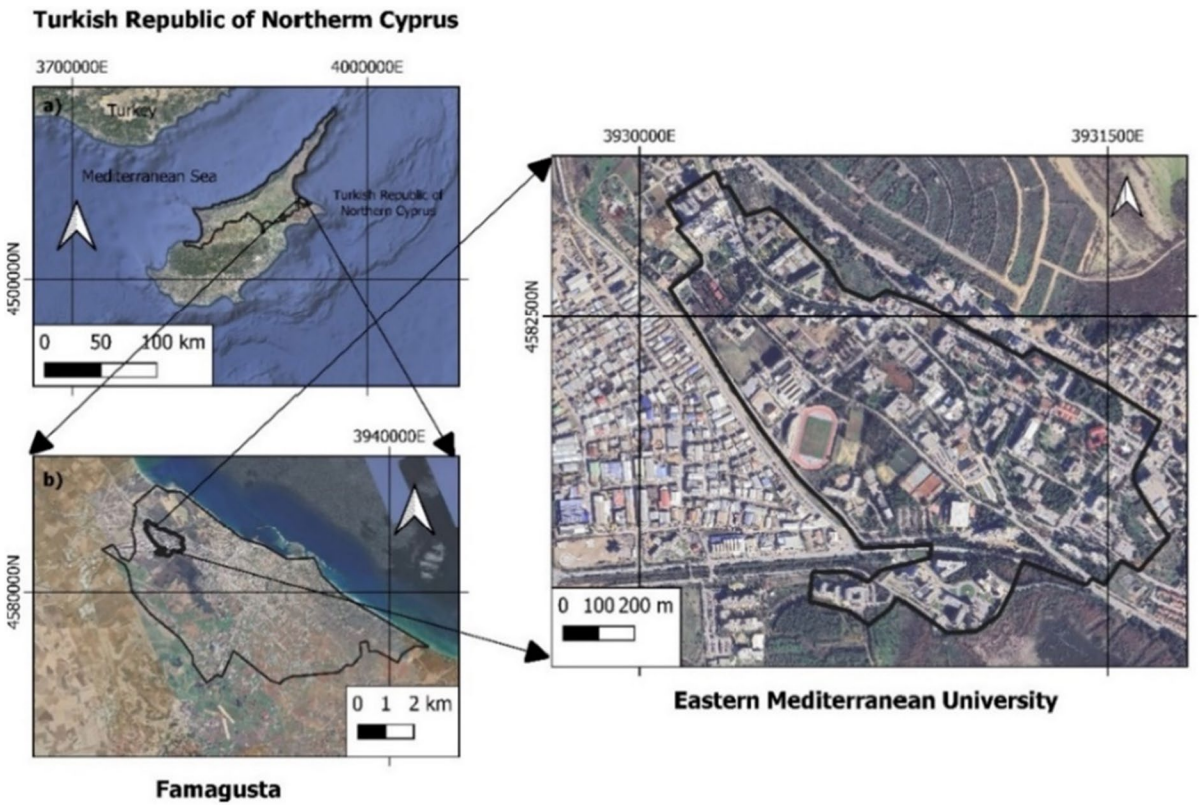

Fig. 1 Study Area, Famagusta; Northern Cyprus

Fig. 2 EMU Campus

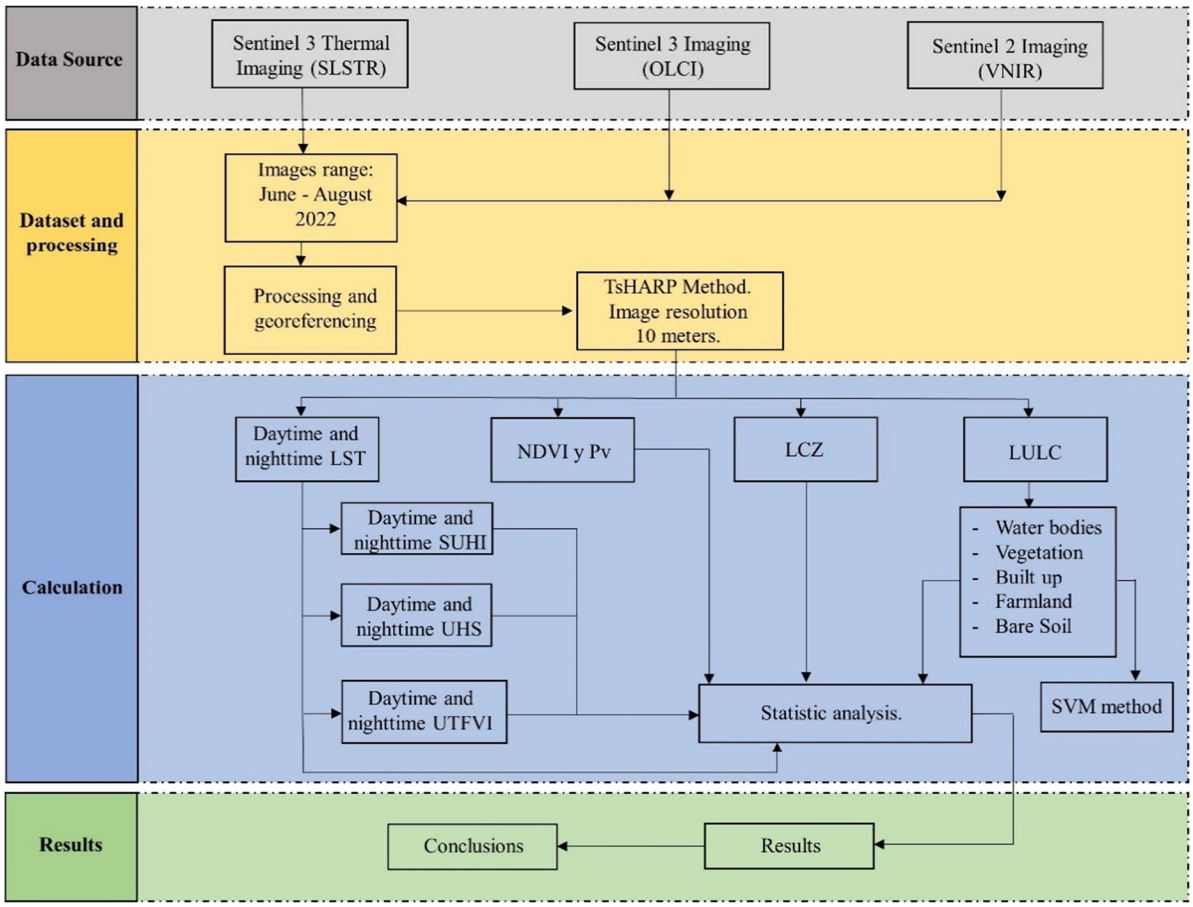

Fig. 3 Methodology

resolution of 500 m. Using the open source software SNAP, Sentinel 3 thermal images of the Earth's surface were obtained at a resolution of 1000 m. An atmospheric correction and band reclassification process was applied and the images were resampled with a resolution of 10 m using the TsHARP algorithm using the PV and NDVI images from Sentinel 2 as a basis (Belgiu & Stein, 2019). Subsequently, and in order to characterize the Earth's surface, urban areas were classified into different LCZs (Stewart & Oke, 2009). Using the QGIS software, the SUHI, UHS, and UTFVI were determined and subsequently, the

data were analyzed statistically using the STATA software, version 16.

2.3 Classification of LCZ.

The area under study was classified using different LCZs (Stewart & Oke, 2009). These are areas that have the same coverage, characteristics and building density in order to allow cataloging of Earth's surface. Each LCZ has its own specific properties and characteristics (Stewart & Oke, 2012). This classification has been used in numerous studies (Qiu et al., 2020; Stewart, 2011) to obtain the different LULCs and their climatic variables, such as LST and SUHI (Brousse et al., 2019; Equere et al., 2020). Therefore, its use has the objective of characterizing the landscape through a classification used worldwide and that allows the results obtained in each LCZ to be extrapolated to the rest of the cities.

Firstly, the city was classified into the different LCZ typologies according to the description of the authors Stewart and Oke (2012). Eleven LCZ were obtained: bushes, bare soil, sparsely built, scattered trees, bodies of water, compact and open of medium and low height. -Boom and heavy industry, and EMU Campus (Fig. 4). The steps carried out to obtain these LCZ are as follows: (1) Collection of metadata for each area based on high-resolution images from the Sentinel 2 and Google Earth satellites (Yang et al., 2019). (2) These images were compared with the LCZ images obtained. (3) Realization of the definitive delimitation of each LCZ. (4) Cataloging of the different LCZ obtained. In general terms, the LCZ obtained had values similar to those referenced by the authors Stewart and Oke (2009).

In the comparison between Sentinel 2 and LCZ images obtained, it was reported that only three of the 50 control points did not coincide. Therefore, a manual correction was carried out in order to determine a high degree of agreement, which finally reached 94%.

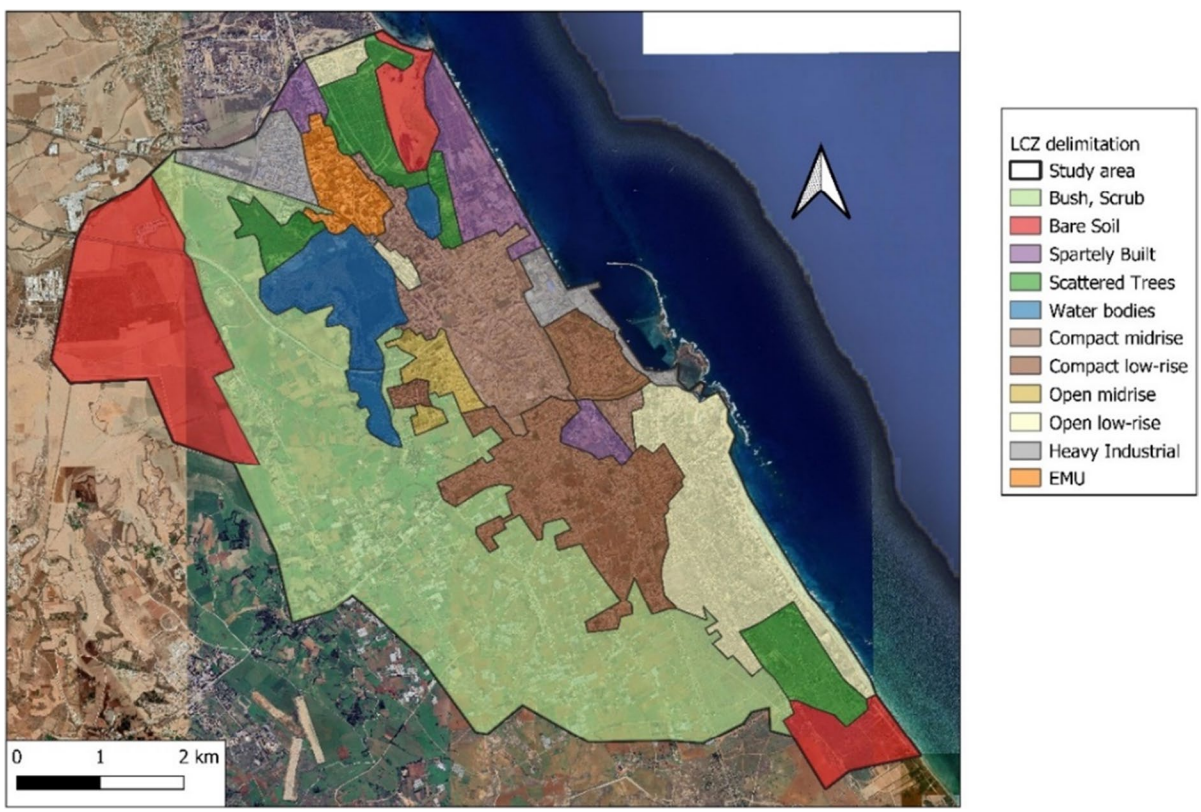

Fig. 4 LCZ of the area under study

2.4 Sentinel 2 Images

Sentinel 2 provides multispectral images of the Earth's surface at a resolution of 10 m. This allows us to observe the possible alterations or modifications that occur on the Earth's surface at any point on the planet. Each Sentinel 2 image has 12 spectral bands with resolutions ranging between 10 and 60 m. Our research used a total of twelve images (6 daytime and 6 nighttime). All of them were carried out during the months of July and August 2022. The images were obtained from the Copernicus Open Access Hub level 2 program. This consists of a repository owned by the ESA (ESA).

2.4.1 LULC

In order to obtain the LULC plans of the ground, bands 2 (red), 3 (green) and 4 (blue) (RGB) of Sentinel 2 were used. Next, and using the QGIS software and the SVM, the city was classified. and the EMU campus and the LULC coverage planes were obtained in raster images (Amindin et al., 2021; Otukei & Blaschke, 2010).

2.4.2 NDVI

With the red (R) and near-infrared (NIR) bands, the NDVI was calculated. Through this index, the presence of vegetation on the soil can be visualized. NDVI values range between -1 (light soils and sparse vegetation) and 1 (dense vegetation) (Amindin et al., 2021):

$$\mathrm{NDVI} = \frac{\mathrm{NIR} - \mathrm{Red}}{\mathrm{NIR} + \mathrm{Red}} \tag{1}$$

With the results obtained in Eq. 1, the PV can be calculated using Eq. 2 (Yu et al., 2014). This allows establishing the proportion of existing vegetation in an area (Rajeshwari A, 2014):

$$\mathrm{PV} = \left[\frac{\mathrm{NDVI} - \mathrm{NDVI}_{\mathrm{min}}}{\mathrm{NDVI}_{\mathrm{max}} - \mathrm{NDVI}_{\mathrm{min}}}\right]^2 \tag{2}$$

where NDVI max and NDVI min are the maximum and minimum values of the NDVI interval, and NDVI is the normalized vegetation index obtained by Eq. 2.

2.5 Sentinel 3 Images

Using the Sentinel 3 images, the surface temperature can be obtained since they have 3 thermal bands with a pixel size of 1000 m and 6 bands (S1 to S6) with a resolution of 500 m. NDVI and PV images are included directly and associated with thermal images within Sentinel 3 level 2 products.

The study area is accessible through Sentinel 3 images. Sentinel 3A's transit time is from 11:00 a.m. to 12:00 p.m., while Sentinel 3B's transit time is from 10:00 p.m. to 11:00 p.m. Six daytime images and another six nighttime images matching the Sentinel 2 images have been selected. These have a cloud index of less than 5%. The images used have been acquired from ESA for level 2. The correction process carried out has been the same as for Sentinel 2 images.

2.6 Image Reclassification using the TsHARP Algorithm

Since Sentinel 3 images have a resolution of 1000 m and given the need to have high resolution images, in recent years different techniques or methodologies have been carried out that allow images to be transformed from low to high resolution. Among these methods, the following stand out: Distrad, STARFM and TsHARP. All of them allow for improving the resolution of the images through an interpolation method with others that do have better resolutions such as NDVI and PV images. The most used method due to its simplicity, excellent results and precision is the TsHARP algorithm (Agam et al., 2007; Zhou et al., 2020). This uses a linear correlation model based on the direct relationship that numerous authors have reported between LST and PV. It is calculated using formula 3:

$$\mathrm{LST}_{\mathrm{coarse}} = \mathrm{a} + \mathrm{b} \times \mathrm{PV}_{\mathrm{coarse}} \tag{3}$$

$\mathrm{PV}_{\mathrm{coarse}}$ and $\mathrm{LST}_{\mathrm{coarse}}$ represent the PV and LST determined using Sentinel 3 imagery at 1000 m resolution. The regression coefficients are the variables "a" and "b" and are determined by statistical analysis. Next, we use Eq. 4:

$$\mathrm{LST}_{\mathrm{fine}} = \mathrm{a} + \mathrm{b} \times \mathrm{PV}_{\mathrm{fine}} \tag{4}$$

$\mathrm{PV}_{\mathrm{fine}}$ comes from Sentinel 2 images that present a resolution of 10 m. Next, $\mathrm{LST}_{\mathrm{fine}}$ comes from the LST derived at 10 m resolution. The coefficients

"a" and "b" have been determined through statistical analysis. Finally, it is mandatory in all statistical analysis to add the residual error (residual) in order to increase precision. All this, according to Eq. 5:

$$LST_{downscale} = LST_{fine} + Residual \quad (5)$$

2.7 SUHI Estimation

The SUHI is characterized by temperature disparities between urban and rural regions measured concurrently (Oke, 1987), as described by Eq. 6:

$$SUHI = LST_{urban} - LST_{rural} \quad (6)$$

The urban LST has been obtained with the pixels located in urban areas, while the rural LST has been determined with the value of the LCZ pixels classified as Scattered Trees. These are located at an adequate distance from urban areas and do not have paved areas around them. Using day and night LST images from Sentinel and using the equation, Eq. 6 can be obtained.

2.8 UHS Estimation

From the LST within the study area, the UHS hot spots are located. They are areas within the high temperature zones and are usually uncomfortable for people. These zones are located using the following Eq. 7 (Guha, 2017; Sharma et al., 2021):

$$LST > \mu + 2 * \sigma \quad (7)$$

σ and μ are the standard deviation and the mean values of the LST in K, respectively. By applying this formula, hot urban areas with LST values higher than the mean values in a 95% confidence interval are located.

2.9 UTFVI Estimation

SUHI generates a significant impact on the quality of life in urban areas. The impact of the SUHI is measured and valued through the UTFVI index that compares the temperature of each pixel with the average values of the entire surface (Guha et al., 2018). This generates a scale of six classes and six indices (Liu & Zhang, 2011) of ecological evaluation (Table [9]). The six ecological evaluation indices are organized according to the strength of the SUHI and have a range between excellent and worse. The UTFVI index is calculated Eq. 8 (Guha et al., 2018):

$$UTFVI = \frac{LST - T_{mean}}{T_{mean}} \quad (8)$$

where T_{mean} is the average LST of the entire area (K) and LST is the temperature of each pixel (K). Through the day and night LST, the day and night UTFVI indices of the area under study have been determined. The absence of the SUHI effect is indicated by values below zero in the UTFVI. They correspond to maximum comfort or excellent quality. As UTFVI values increase, thermal comfort deteriorates (Sharma et al., 2021) due to an increase in SUHI.

2.10 Strategy of Analysis

The statistical analysis used two methodologies: ANOVA and Panel Data. The first allows us to compare the variances between the means of the different groups in order to check if there are statistically significant differences. For that means, an ANOVA has been used with a dependent variable (LST) and an independent variable (LCZ). Some already published studies have used this methodology in similar research (Safarrad et al., 2021; Sharma et al., 2022). Secondly, the Data Panel allows us to obtain better results in analyzes that have cross-sectional and time data (Alcock et al., 2015; Fang & Tian, 2020). To carry out this last analysis, the steps described in Chen et al., (2011) have been followed. This was done using the STATA software following Eq. 9:

$$Y_{it} = \beta X_{it} + (\alpha_i + \mu_{it}) \quad (9)$$

where β is an independent variable, Xit are explanatory variables, μ_{it} is the error of the model and α_i represents the individual effects.

3 Results

3.1 NDVI and PV Indices

Figure 5 illustrates the PV and NDVI indices. NDVI is a metric that gauges the health and condition of

vegetation covering the Earth's surface, whereas PV reflects the relative amount of vegetation in a given area in contrast to urbanized regions. In Fig. 5a, the NDVI index demonstrates an average range fluctuating between its highest value (0.2972), observed in green regions, and its lowest value (0.1500), found in urban and non-vegetated rural areas. The overall average NDVI value across the entire study area was calculated as 0.184. In Fig. 5b, the PV index displays an average span varying between its peak value (0.1300), noted in green and open urban regions, and its lowest value (0.0170), observed in densely populated urban areas and non-vegetated rural zones. The average PV value for the entire study area was computed as 0.0722. The acquired NDVI values suggest that the vegetation in the study area is suitable for the summer period. On the other hand, the PV values report that the city has few areas of vegetation and a dispersed location.

Table 1 displays the mean PV and NDVI values within each LCZ.

Specifically, the NDVI index exhibits its highest values in the Scattered Trees (0.2105), EMU Campus (0.1953), and Bare Soil (0.1920) zones, while the lowest values are observed in the Water Bodies (0.1678), Bush and Scrub (0.1728), and Heavy Industrial (0.1746) areas. Conversely, the PV index registers its highest values in the Scattered Trees (0.0844), Bush and Scrub (0.0840), and Water Bodies (0.0705) zones, while the lowest values are found in the Compact Midrise (0.0376), Heavy Industrial (0.0426), and Open Low-Rise (0.0453) zones.

Table 1 Index NDVI and PV of the area investigated by LCZ

LCZ	NDVI	PV
Compact Mid Rise	0.1763	0.0376
Compact Low Rise	0.1826	0.0496
Open Mid Rise	0.1816	0.0626
Open Low Rise	0.1856	0.0452
Heavy Industrial	0.1746	0.0426
Bush, Scrub	0.1728	0.0841
Bare Soil	0.1923	0.0442
Sparsely Built	0.1846	0.0457
Scattered Trees	0.2105	0.0884
Water bodies	0.1678	0.0705
EMU Campus	0.1953	0.0878
Mean	0.1841	0.0722

Figure 6 shows the average values of the NDVI and PV indices by area: urban, rural, EMU and heavy industrial. In this way, the highest NDVI value is located in the EMU campus area (0.1953) while the lowest value is located in the heavy industrial area (0.1746). The highest value of PV is located in the rural zone group (0.0718) while the lowest value is located in the heavy industrial area (0.0426). From these results, the extensive development of green areas located within the EMU campus is corroborated, being an important factor in the control of high temperatures in the city.

The outcomes of the ANOVA test conducted on the NDVI and PV indices have revealed that these data do not conform to normal distributions across

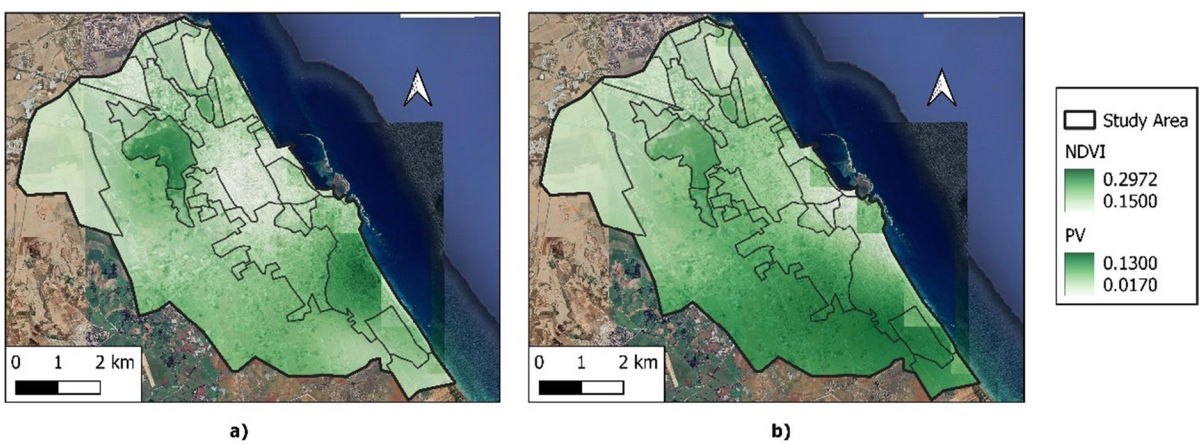

Fig. 5 Index **a**) NDVI and **b**) PV of the area under study

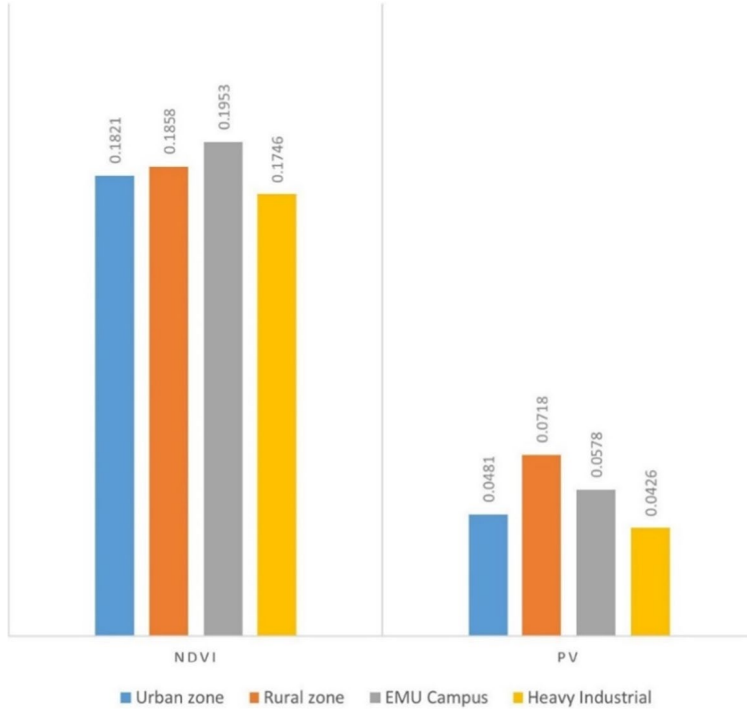

Fig. 6 Mean index values **a**) NDVI and **b**) PV of the investigated area

Table 2 ANOVA test results between the NDVI, PV and LCZ indices

Source	NDVI	PV
Difference of Square	*0.0001****	*0.0001****
R^2	52.03	48.63

F: Statistical. R^2: Linear regression coefficient.

various LCZs, as indicated by the Shapiro–Wilk test with p-values less than 0.05. Consequently, to proceed with the analysis under non-normal distribution conditions, the Kruskal–Wallis test was executed, and the resulting findings are presented in Table 2.

Hence, based on the reported results, it can be concluded that the values of the PV and NDVI indices exhibit statistically significant relationships between the various LCZs at a significance level of above 99%.

3.2 Evaluation of the LULC

The coverage of the LCZ taken into account is represented in Fig. 7 and 8. Regarding the average values, the coverage with the largest area in the city of Famagusta is the Built up (54.1%) while the coverage with smaller surface is the vegetation (10.8%). Bare soil coverage (17.3%), farmland (17.7%) and water bodies (10.9%) are found with intermediate values. Figure 9 shows the different coverages by LCZ. The compact midrise (90.2%) and heavy industrial (89.7%) zones present a higher average proportion of built-up coverage. On the contrary, the bare soil (18%) and bush, scrub (19.1%) areas present the lowest average proportion of this coverage. These results are in line with those obtained for the NDVI and PV indices in the previous section.

It is important to note how the compact areas of the city have a higher average built-up coverage (73.5%) than the open areas (62.2%). However, the average vegetation cover is also higher in compact areas (12.85%) as opposed to open areas (10.6%). However, the latter present a greater coverage of farmland (16.9%) than the compact zones (8.6%). Therefore, the non-built-up areas of the open areas are intended for vegetation and, to a greater extent, for farmland.

Figure 9 shows the different investigated coverages grouped by zones: rural, urban, heavy industrial and EMU campus. It can be seen how the heavy industrial area has a very low vegetation coverage (0.3%) while the majority coverage is built up (89.7%). The

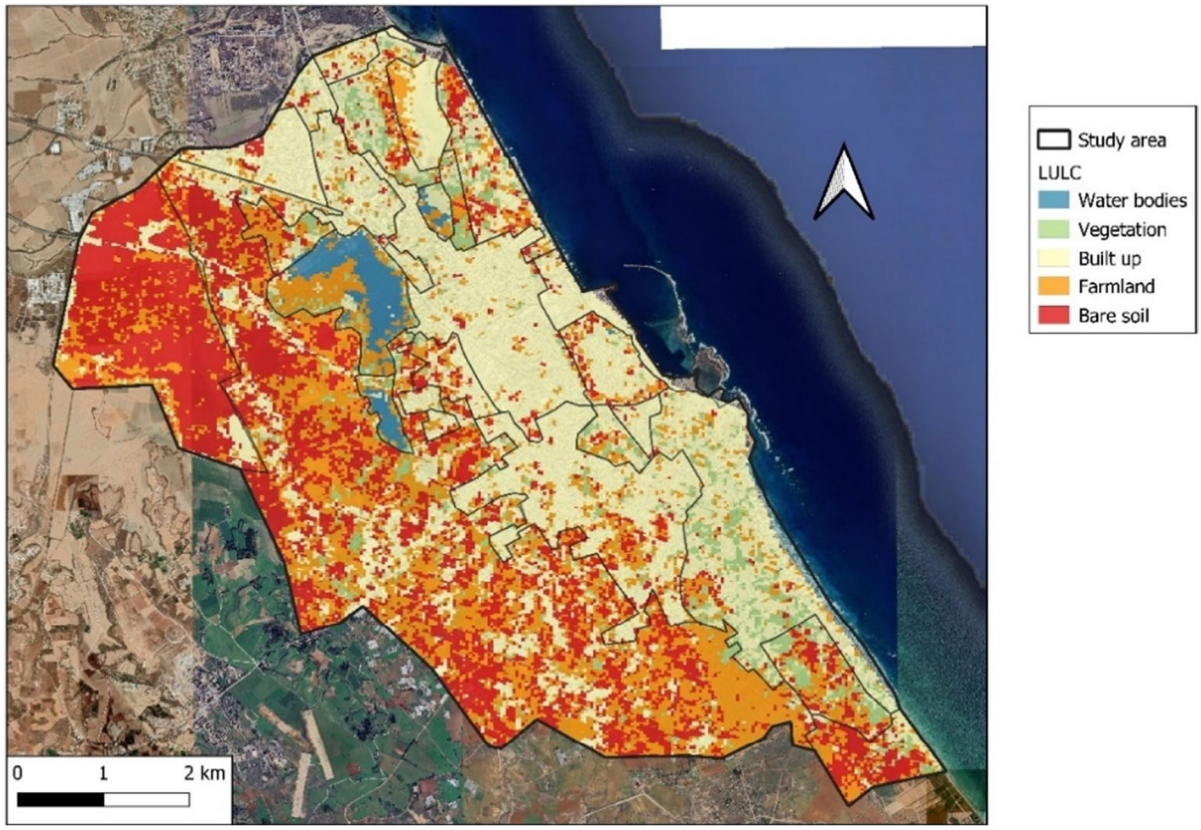

Fig. 7 LULC coverage of the area Under study

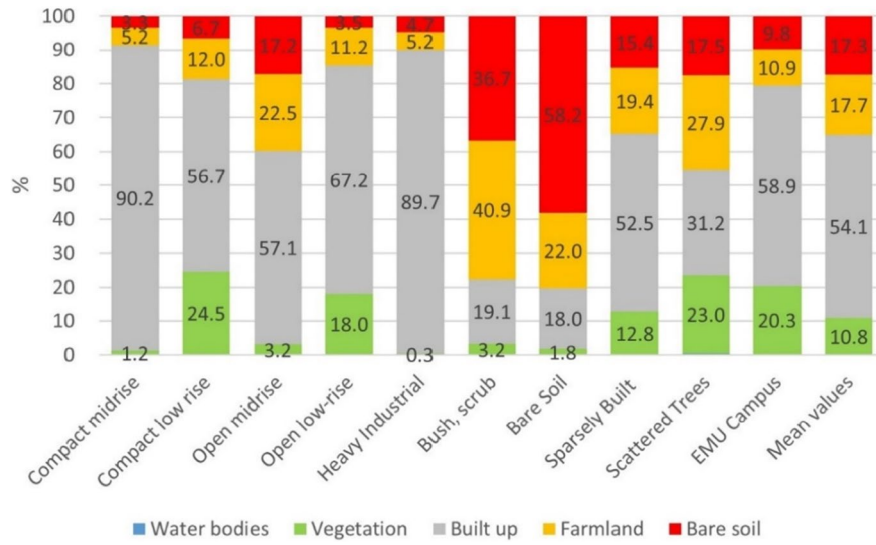

Fig. 8 Average LULC values in the different LCZ

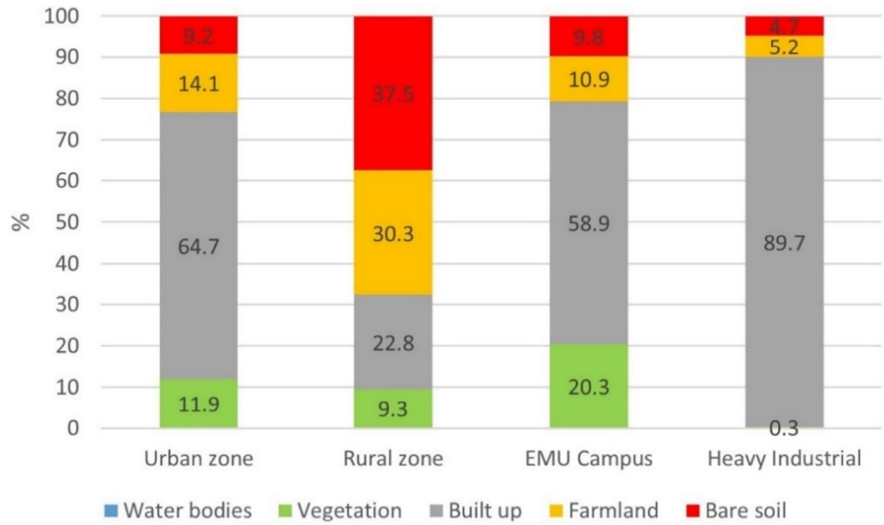

Fig. 9 Average LULC values by zones

farmland (5.2%) and bare soil (4.7%) coverages also have very low surfaces. In the rural zone, the greatest coverage is bare soil (37.5%) followed by farmland (30.3%), built up (22.8%) and vegetation (9.3%). In the urban areas of the city of Famagusta, built up coverage stands out (64.7%) followed by farmland coverage (14.1%), vegetation (11.9%) and bare soil (9.2%). With regard to the EMU campus area, the area devoted to vegetation (20.3%) is higher than the rest of the areas and the built-up coverage (58.9%) is lower than the rest of the urban areas. These results are in line with the values reported in the previous sections for the NDVI and PV indices.

Table 3 shows the results of the precision matrix. The global precision has been 84.74% with a confidence interval of 95%. The Tau coefficient is 0.791 and the Kappa coefficient is 0.808. After determining these results, a manual correction of the points has been made.

The outcomes of the ANOVA test performed on LULC data have indicated, based on the Shapiro–Wilk test with a P value greater than 0.05, that these data follow a normal distribution within the various LCZs. The results presented in Table 4 confirm the presence of statistically significant differences exceeding the 99% confidence level among the means of the distinct land cover categories and the different LCZs under investigation. The statistic $F > 0$ and the variable $Prob > Chi^2 < 0.001$ further support this conclusion.

3.3 Spatio-temporal evaluation of LST

Figure 10 shows the distribution of daytime and nighttime LST. During the mornings, the maximum value of LST was 323.7 K while the average value was 318.5 K and the lowest value was 311.1 K. The difference in daytime LST within the EMU campus was 5.3 K. Figure 11a illustrates the phenomenon where urban areas exhibit lower LST values compared to the higher temperatures observed in rural areas. This phenomenon can be attributed to several

Table 3 Precision matrix

	Water bodies	Vegetation	Built up	Farmland	Bare soil	UA (%)
Water bodies	10	0	0	0	0	100
Vegetation	0	10	0	0	0	100
Built up	1	0	10	1	2	60
Farmland	0	0	5	10	0	50
Bare soil	0	0	0	0	10	100
PA (%)	90	100	50	90	80	50

UA (5): User accuracy. PA (5): Producer Accuracy

Table 4 ANOVA test results between LULC and LCZ

Source	LULC
Sum of Square	39.5268
Df	10
Mean of Square	3.9526
F	5.11
Prob > Chi^2	*0.000****
R^2	0.269

F: Statistical. R^2: Linear regression coefficient.

factors. One significant factor is the higher solar radiation received in rural areas during the morning hours, which surpasses the radiation received in urban areas. This difference is a consequence of the shading effect produced by buildings and vegetation in urban areas, which limits the heating of impermeable surfaces such as streets. Additionally, vegetated areas in rural regions experience more efficient cooling processes, contributing to lower temperatures (Lemus et al., 2020). During the nights, the maximum value of LST has been 299.6 K while the average value has been 298.2 K and the lowest value has been 297 K. The difference of night LST within the EMU campus has been 1.9 K. Figure 11b shows how the highest values of LST are located in the interior of the city, while rural areas have lower values of LST. This is because urban areas tend to cool more slowly than rural areas once the sun goes down, as they retain heat. The waterproof construction materials used in cities absorb heat from solar radiation, and at night, after the sun goes down, they release it, heating up the atmosphere (Hidalgo García and Arco-Díaz, 2022).

In Fig. 11, the mean day and night LST are represented by LCZ. It can be seen how the highest daytime LST is located in the bush, scrub (320.5 K) and bare soil (317.2 K) zones, while the lowest LST values are located in the water bodies (313.6 K), EMU Campus (314.5 K) and open low-rise (314.9 K). During the nights, the highest LST is located in the compact midrise (299.1 K) and open midrise (298.8 K) zones, while the lowest values are located in the bare soil (297.3 K), scattered trees (297.7 K) and EMU Campus (297.8 K).

Figure 12 shows the mean daytime and night-time LST by area: urban, rural, EMU campus and heavy industrial. In this way and during the mornings, the highest LSTs are found in the rural zones (316.5 K) as opposed to the lowest LSTs that are located in the EMU campus area (315.1 K). The urban areas have presented an average LST of 315.6 K and the heavy industrial areas an LST of 315.9 K. On the contrary, and during the nights, the highest LST is located in the urban zones (298.6 K) while the lowest LST they are located in rural areas (297.6 K). The areas classified as heavy industrial have an average nighttime LST of 298.2 K and the EMU Campus an LST of 298 K. In this way, it can be seen how the EMU Campus has the lowest daytime LST of the areas studied while it has the lowest LST lowest nightlife in urban and industrial areas. This is due to the urban planning

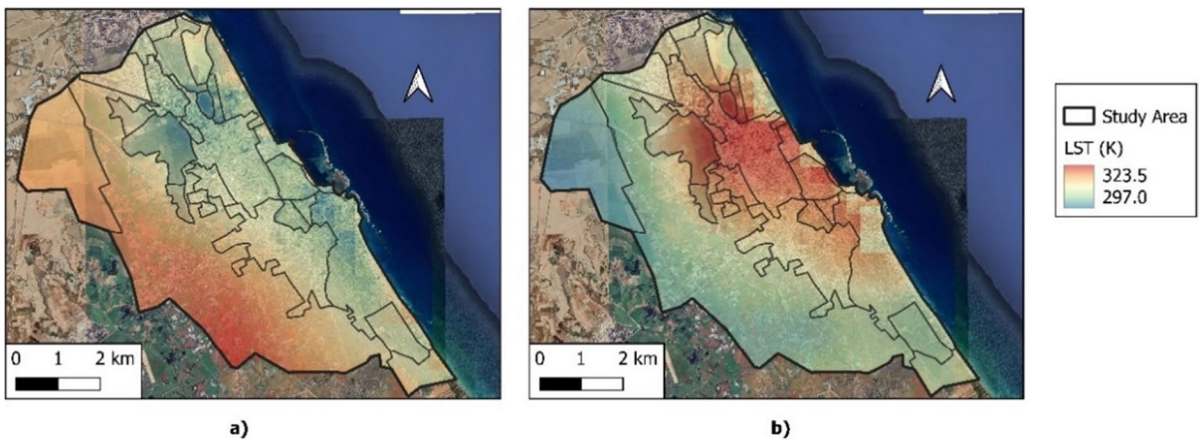

Fig. 10 LST a) daytime and b) night-time of the area under study

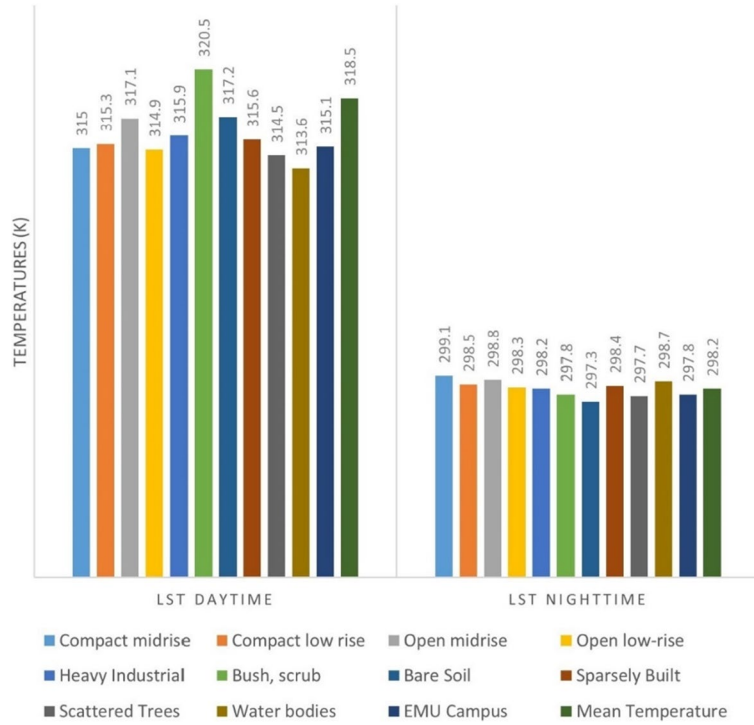

Fig. 11 LST daytime and night-time by LCZ

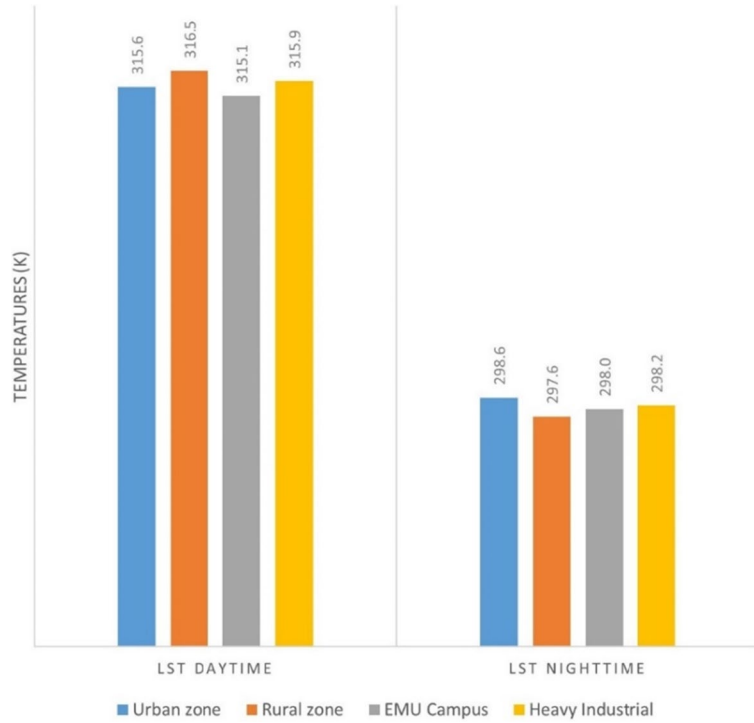

Fig. 12 Average LST daytime and nighttime by area

that presents the campus with low-rise buildings and large open spaces with vegetation that generate shadows in the morning and high percentages of cooling at night. There are numerous investigations that report significant cooling rates in urban areas that have extensive green areas (Hidalgo, 2023).

The outcomes of the ANOVA test conducted on LST data have revealed, based on the Shapiro–Wilk test with a P-value less than 0.05, that these data do not conform to normal distributions across different LCZs. Consequently, to proceed with the ANOVA test under the assumption of non-normal distributions, it was essential to perform the Kruskal–Wallis test. The results of this test are presented in Table 5.

Hence, based on the reported results, it can be concluded that the LST values exhibit statistically significant relationships exceeding the 99% confidence level across different LCZs. To determine the relationships between LST and the PV, LULC, and NDVI indices within the study area, the Data Panel method will be employed. This approach allows for a comprehensive analysis of the interactions and dependencies among these variables, taking into account both time and value data.

In Table 6 it can be seen how temperatures have a significant negative correlation with NDVI (-0.1935) and PV (-0.2742) and positive with LULC (0.3246).

The following results are reported (Table 7) statistically significant relationship above 99% between temperatures and LULC, greater than 99% and negative with the PV variable and 99% and negative with the NDVI variable. In summary, areas with higher PV and NDVI values tend to have lower temperatures, whereas areas with lower PV and NDVI values exhibit higher temperatures. Additionally, it's worth noting that changes in LULC coverage are associated with temperature variability, indicating a connection between urban development and temperature patterns.

sd: Standard deviation; F: Statistical. R^2: Linear regression coefficient; β: Coefficient.

Table 5 ANOVA test results between the LST and LCZ

Source	LST
Difference of Square	*0.0001****
R^2	61.76

F: Statistical. R^2: Linear regression coefficient.

Table 6 Correlation coefficient

	LST	PV	NDVI	LULC
LST	1			
PV	-0.2742	1		
NDVI	-0.1935	0.2280	1	
LULC	0.3246	0.0342	-0.1664	-0.8831

3.4 SUHI Spatio-Temporal Evaluation

Figure 13 shows day and night SUHI in the city of Famagusta.

During the mornings, the maximum value of SUHI has been 7.5 K while the average value has been 2.2 K and the lowest value has been -5.1 K. The difference in daytime SUHI within the EMU campus was 5.2 K. Figure 14a shows how the highest SUHI values are located in rural areas as opposed to the lowest SUHI values that are located in urban areas. The diurnal SUHI difference within the EMU campus has been 5.2 K. In Fig. 14a, During the nights, the maximum value of SUHI has been 1.7 K while the average value has been 0.3 K and the lowest value has been -0.9 K. The difference in nocturnal SUHI within the EMU campus was 0.9 K. Figure 14b shows how the highest values of SUHI are located in the interior of the city while rural areas show higher values. lower than SUHI. In Fig. 14, the mean daytime and nighttime SUHI are represented by LCZ. It can be seen how the highest daytime SUHI is located in the Bush, scrub (4.3 K) and bare soil (1.1 K) zones, while the lowest LST values are located in the water bodies (-2.6 K) and scattered zones. trees (-1.7 K). During the nights, the highest SUHI is located in the compact midrise (1.1 K) and open midrise (0.9 K) zones, while the lowest values are located in the bare soil (-0.7 K) and water bodies (-0.2 K) zones.

Table 7 Data Panel results

	β	ρ	sd
NDVI	-18.5793	*0.006***	6.6853
PV	-28.9176	*0.000****	7.1469
LULC	1.15046	*0.000****	1.2355
	$R^2 = 0.22$	*F = 12.78*	Prob > $chi^2 = 0.000$

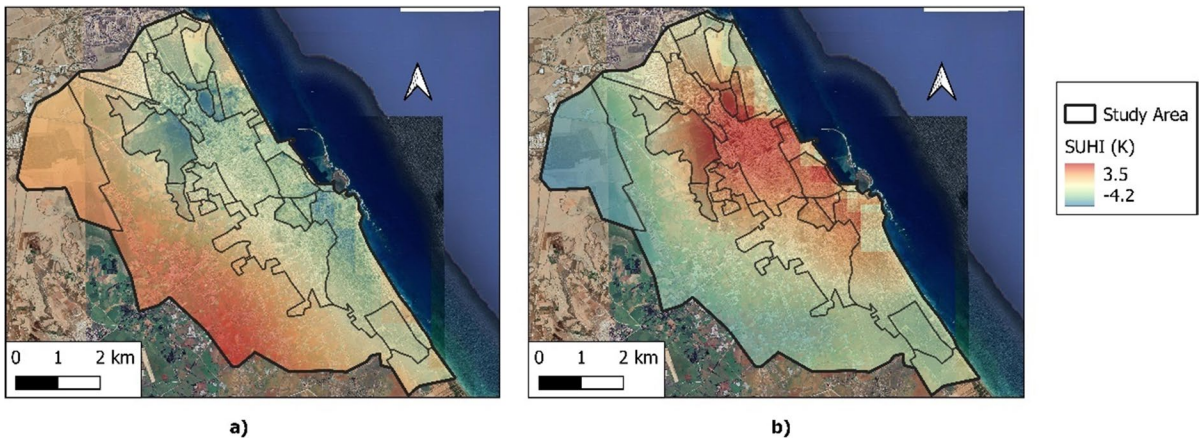

Fig. 13 SUHI **a**) daytime and **b**) nighttime of the area Under study

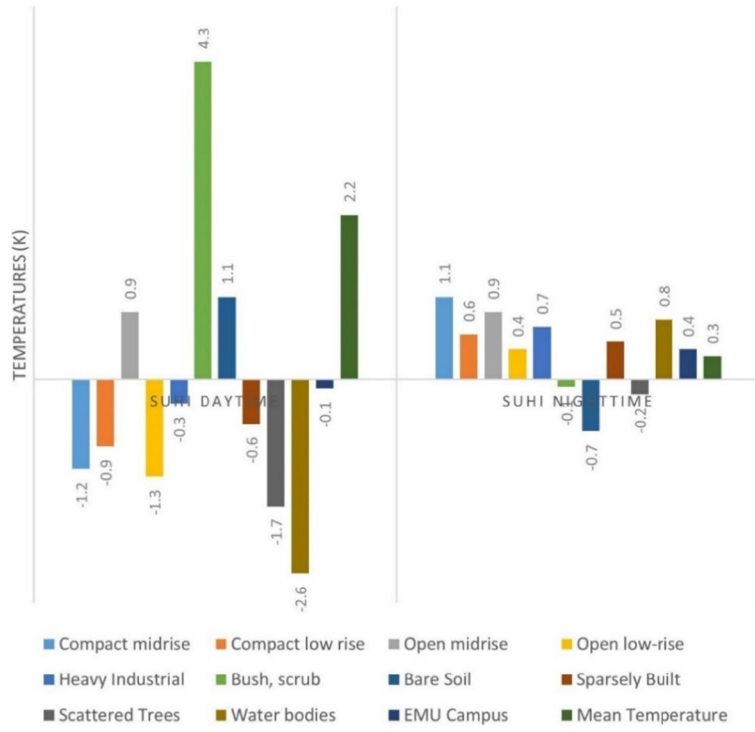

Fig. 14 SUHI daytime and nighttime by LCZ

Figure 15 shows the average day and night SUHI by areas: urban, rural, EMU campus and heavy industrial. In this way and during the mornings, the highest SUHIs are found in the rural zones (0.3 K) as opposed to the lowest SUHIs that are located in the urban zone (-0.8 K). Both the heavy industrial (-0.3 K) and EMU campus (-0.1 K) zones present SUHI with negative values, respectively. This situation reveals that rural areas have higher temperatures than urban ones during the mornings. This situation is identified as an urban cooling island (García & Díaz, 2023; Yang et al., 2020a, b). On the contrary, and during the nights, the highest SUHIs are located in the urban (0.7 K) and heavy industrial (0.7 K) areas,

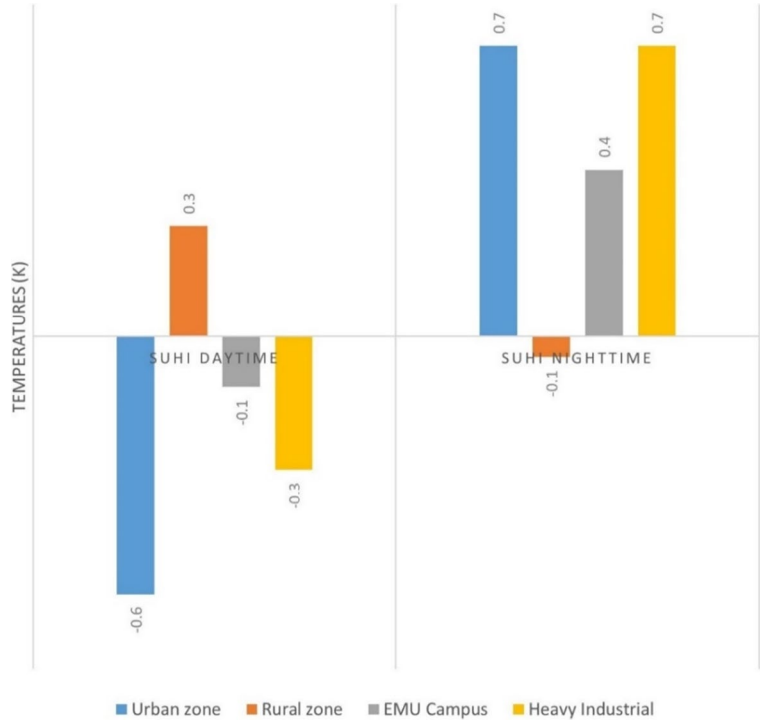

Fig. 15 Average SUHI daytime and nighttime by area

while the lowest SUHI values are located in the rural area (-0.1 K) and EMU campus (0.4 K). This circumstance suggests that rural areas have lower temperatures than urban areas at night. Numerous authors have reported this situation, identifying it as an urban heat island (Hidalgo García and Arco Díaz, 2021; Yang et al., 2020a, b). It is observed how the campus EMU zone presents lower day and night SUHI than the urban zones. This situation is once again motivated by the urbanism that the campus presents with low-rise buildings and large open spaces with vegetation that generate shadows in the morning and high cooling percentages at night. Numerous investigations report a minimization of temperatures in urban areas with large areas of green cover.

The outcomes of the ANOVA test conducted on the SUHI data have indicated, as per the Shapiro–Wilk test with a P-value less than 0.05, that these data do not adhere to normal distributions across different LCZs. Consequently, in order to proceed with the ANOVA test under the assumption of non-normal distributions, it was imperative to conduct the Kruskal–Wallis test. The results of this test can be found in Table 8.

According to the reported results, it can be inferred that the SUHI values demonstrate statistically significant relationships exceeding the 99% confidence level across different LCZs. Subsequently, employing the Data Panel method will help determine and explore the relationships between SUHI and various factors within the study area.

Table 9 shows how the SUHI presents a strong negative correlation with the NDVI (-0.1598) and PV (-0.3017) indices and positive with the LST (0.8434) and LULC (0.4729). The results report the following results (Table 10) a relationship greater than 99% and statistically significant positive between LST and SUHI and LST and LULC, greater than 99% and negative with the PV variable and 95% and negative with the NDVI variable

Table 8 ANOVA test results of the SUHI between the LCZ

Source	SUHI
Difference of Square	*0.0001****
R^2	78.97

F: Statistical. R^2: Linear regression coefficient.

Table 9 Pearson`s correlation

	SUHI	LST	NDVI	PV	LULC
SUHI	1				
LST	0.8434	1			
NDVI	-0.1598	-0.1935	1		
PV	-0.3017	-0.2742	0.2280	1	
LULC	0.4729	0.3246	-0.1664	0.0342	1

Table 10 Data Panel results

	β	ρ	sd
LST	0.5836	*0.000***	0.0369
NDVI	-10.7067	*0.029**	5.1867
PV	-23.2890	*0.000***	5.1867
LULC	1.04483	*0.000***	0.1709
	$R^2 = 0.33$	*F* = *22.41*	Prob > $chi^2 = 0.000$

sd: Standard deviation; F: Statistical. R^2: Linear regression coefficient. β: Coefficient.

3.5 UHS identification

Figure 16 and Table 11 show the UHS during the day (11.95%) and at night (24.77%) in the city. A clear spatial variability can be seen between the areas classified as UHS during the mornings and evenings. Thus, in the former, the UHS is located in rural areas, while at night the UHS is located in the center of the city. This circumstance is motivated by the fact that during the mornings, rural areas without vegetation heat up more quickly than urban areas due to the shadows produced by buildings or trees on the streets. On the contrary, during the night, construction materials that have been heated during the day release heat into the atmosphere, producing the UHI phenomenon.

Table 11 Temperatures for UHS

	Non UHS (K)	UHS (K)	UHS (ha)	UHS (%)
Daytime	< 322.0	≥ 322.0	236.61	11.95
Nighttime	< 299.1	≥ 299.1	489.25	24.77

Figure 17 shows the percentage of occupation of the territory by day and night UHS based on the LCZ. It can be seen how all the daytime UHS are located in the LCZ Bush, scrub, while the night UHS are located mainly in urban areas. Highlight the high occupancy (51%) of the areas classified as compact midrise as UHS during the nights. The EMU campus zone only has 1% of its surface occupied as UHS during the nights. These results denote a construction system, spaces intended for vegetation, and adequate LULC on the part of the EMU university campus that allows for improving the climatic conditions of the adjacent city.

3.6 Evaluation using UTFVI

Figure 18 and Table 12 show the day and night UTFVI evaluation. In general terms and during the mornings, the city presents the vast majority of its

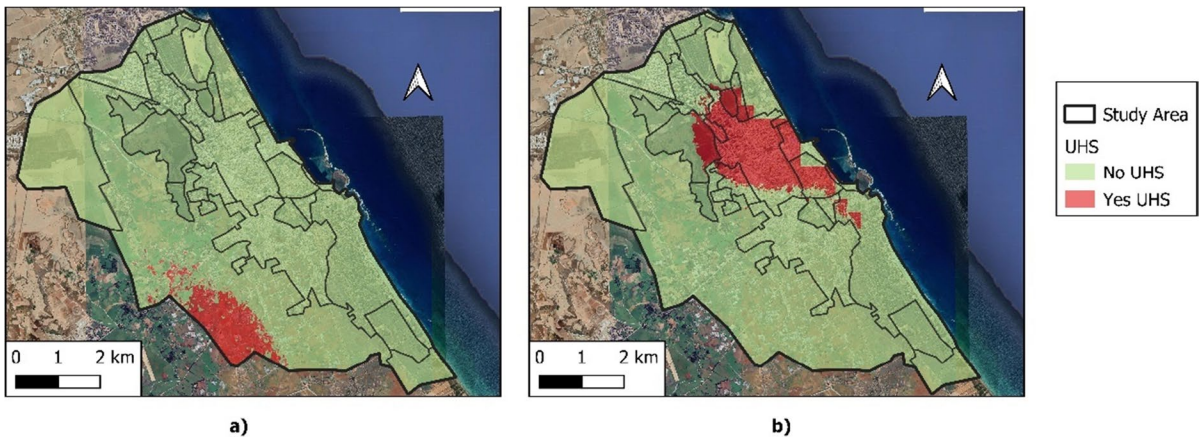

Fig. 16 UHS a) daytime and b) nighttime by area

territory classified according to four UTFVI typologies: class 1 (48.8%), 3 (21.8%), 2 (19.7%), and 4 (9.5%). The areas with the highest rankings are located in urban areas while the areas with the lowest rankings are located in rural areas. On the contrary, during the night, the city presents the great majority of its territory classified according to two UTFVI typologies: class 4 (91.7%) and 3 (7.6%). The areas

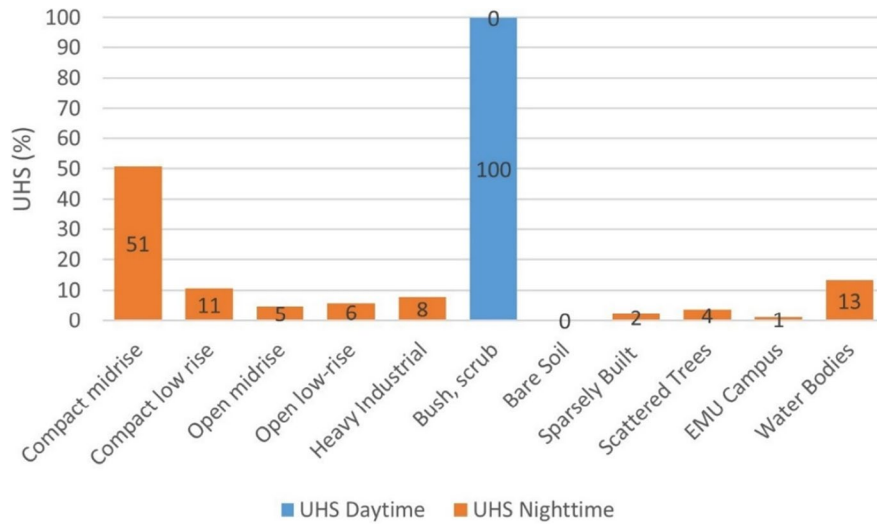

Fig. 17 UHS **a**) daytime and **b**) nighttime by LCZ

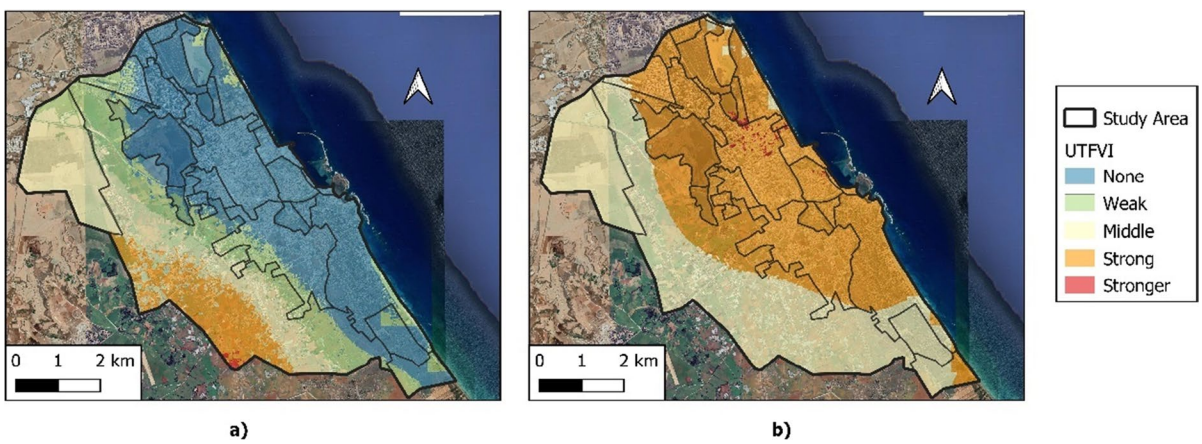

Fig. 18 UTFVI a) daytime and b) nighttime of the area Under study

Table 12 Daytime and nighttime occupation of UTFVI

Class	UTFVI	SUHI presence	Ecological index	Daytime (%)	Nighttime (%)
1	< 0	None	Excellent	48.8	0.0
2	0—0.005	Weak	Good	19.7	0.0
3	0.005—0.010	Middle	Normal	21.8	7.6
4	0.010—0.015	Strong	Bad	9.5	91.7
5	0.015—0.020	Stronger	Worse	0.2	0.8
6	> 0.020	Strongest	Worst	0.0	0.0

with the best rankings are located in rural areas while the areas with the worst rankings are located in urban areas.

Figure 19 shows the occupation of the different classes of UTFVI soil according to the different LCZ in detail. Thus, during the mornings, the heavy industrial and EMU campus areas present 100% of their territory as UTFVI class 1. On the contrary, the Bush, scrub areas present only 10% of the soil as class 1 while class 3 is 34%, class 2 is 31% and class 4 is 25%. In turn, the bare soil zone has 64% coverage classified as UTFVI class 3. During the nights, the Bush, scrub, and bare soil cover are the ones that present the highest % of soil as UTFVI class 1, 76%, and 84%, respectively. The areas with the highest land occupation through UTFVI class 5 are compact midrise (4%) and heavy industrial, scattered trees, and water bodies (1%). The areas with the highest occupancy percentages through UTFVI class 4 are the EMU campus (100%), water bodies (99%), compact midrise (96%), and heavy industrial and sparsely built (91%).

4 Discussion

Our results report that PV and NDVI values, which are indicative of vegetation, exhibit higher values in rural areas compared to urban and industrial areas, where these values are notably lower. Furthermore, when considering the diverse LCZs, it is evident that open areas tend to have higher PV and NDVI values in contrast to compact and industrial zones, where these values are relatively lower. These findings highlight the distinctions in vegetation cover and land use patterns across the different zones within the study area. Therefore, the greater the compactness of the buildings and the building density of the areas, the lower the values in the PV and NDVI indices. From the LULC results, it has been reported that the predominant coverage in urban areas is built up, while in rural areas, it is bare soil. The vegetation cover found is greater in urban areas than in rural areas, being practically nil in industrial areas. Concerning the results of these indices in the EMU campus area, it should be noted that the NDVI and PV indices have been higher than those in the rest of the urban areas, while the predominant coverage has been built up, followed by vegetation. The latter presents an occupation of approximately double that found in urban and rural areas. These results are in line with the spatial distribution and the area designated for green areas that the campus currently presents. These results are in line with those obtained in another research (Avdan & Jovanovska, 2016; Diallo-Dudek et al., 2015; Hidalgo García and Arco Díaz, 2021; Kafy et al., 2021; Wang et al., 2019) allowing us to validate those reported here. However, it is necessary to report that the variability observed in the NDVI and PV indices cannot only be assigned to a territorial planning system carried out by different public organizations but also due to rainfall and irrigation systems (Nicholson & Farrar, 1994). These last variables can contribute greatly to the variability

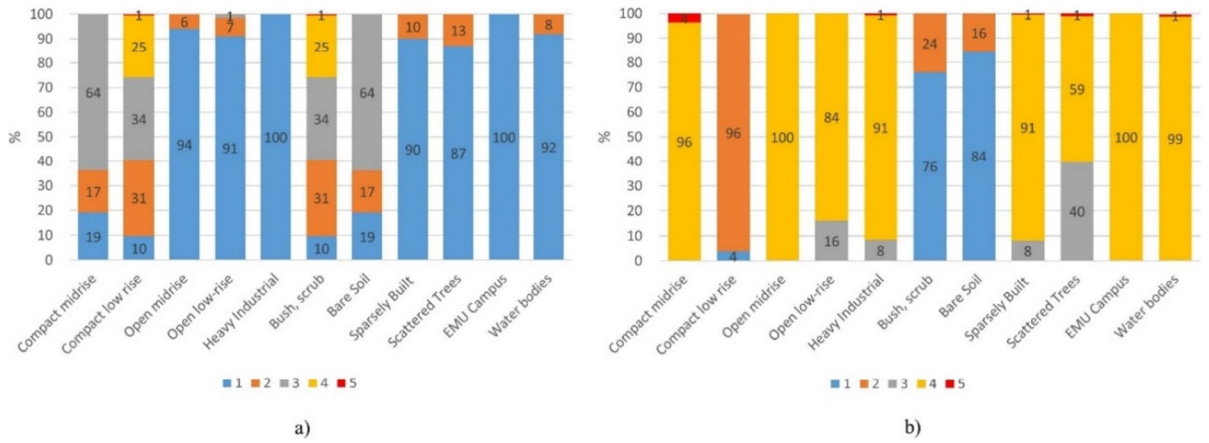

Fig. 19 Occupation of soil classes UTFVI **a**) daytime and **b**) night-time by LCZ

of these factors and therefore this circumstance must be taken into account.

Our results tell us that daytime LST tends to be higher in rural areas and lower in urban areas. In turn, and within the latter, the LST is lower in compact zones than in open and industrial zones. This circumstance could be motivated by the fact that compact areas receive less solar radiation due to the shadows of trees and buildings. Lower radiation allows the waterproof materials with high thermal absorption usually used in the construction processes of cities and buildings not to heat up and therefore allows a reduction in the LST. In this way, it is necessary to report that the more vegetation, the lower the LST, while the less vegetation, the higher the LST. If shadows prevent the entry of solar radiation, the walls will not heat up and heat will not be released (Dwivedi & Mohan, 2018; Lemus-Canovas et al., 2020). In contrast, the average nighttime LST is lower in rural areas compared to urban areas where it is higher. In turn and within the latter, the LST is higher in compact and industrial areas compared to open areas due to the less available vegetation. This is mainly due to the fact that rural areas tend to cool quickly after sunset due to the low thermal inertia of the soil. On the contrary, urban areas retain the heat received during the day from solar radiation due to the high thermal inertia of the materials used. Our results show that the more compact an area is, the more surfaces of impermeable materials it has and therefore, the more heat it retains. The use of waterproof materials with high thermal absorption means that after hiding from the sun, they release the heat absorbed during the day (Saaroni et al., 2018; Suhail et al., 2019; Yang et al., 2020a, b).

Focusing now on the EMU area, it has been reported that during the mornings it has lower LST than the adjacent rural and urban areas. On the contrary, during the night, it has presented lower LST than urban areas but higher than neighboring rural areas. However, important thermal differences have been found within the campus between areas with more and less vegetation. This circumstance is once again motivated by the configuration that the campus presents with low-rise buildings and large green spaces with vegetation. Numerous studies have reported that vegetation has a cooling effect in urban areas (Du et al., 2020; Lin et al., 2015; Qiu et al., 2017), which ranges between 0.5 and 2.5 K. However, the results reported here from LST are below the results reported by other authors (Addas et al., 2020; Cheng et al., 2020; Wibowo et al., 2020) in studies carried out on other university campuses. This circumstance could be mainly motivated by the significant percentage of green areas in the EMU campus with values above those obtained in other campuses. Therefore, it becomes evident that high areas of vegetation in urban areas make it possible to minimize LST and improve the environmental conditions of these areas, improving people's quality of life.

Additionally, an important spatial variability of the diurnal and nocturnal SUHI of the city of Famagusta has been evidenced. The average daytime and night-time SUHI results obtained revealed that the study area experiences an urban heat island since urban temperatures are higher than rural temperatures throughout the day. However, this circumstance must be analysed since the daytime temperatures of the urban LCZ have been lower than the daytime temperatures of the rural LCZ. Therefore, although the average daytime SUHI is positive if we analyse only urban areas, the average SUHI obtained has a negative value. This circumstance is defined as an urban cooling island and has been studied and corroborated by numerous investigations (Hidalgo García and Arco Díaz, 2021; Saaroni et al., 2018; Wu et al., 2019). The mean daytime SUHI according to the LCZ seems to indicate that the open zones present higher intensities than the compact zones. This circumstance changes during the night when compact and industrial areas show higher SUHI intensities than open areas. Chun and Guldmann (2014) reported for the city of Columbia that urban areas with higher densities had higher temperatures than areas with lower densities. This is because the former and due to the higher altitudes do not have airflow and therefore their cooling effects are considerably reduced. These results, together with the research carried out by other authors (García-Santos et al., 2018; Hu et al., 2020; Saaroni et al., 2018; Sekertekin & Bonafoni, 2020; van Hove et al., 2015) come to support the values obtained in our research. Regarding the UEM campus area, our results indicate that during the mornings an urban cooling island occurs, that is, that the campus is at lower temperatures than the surrounding rural areas. On the contrary, at night an urban heat island occurs, that is, the campus is at

higher temperatures than the surrounding rural areas but with a much lower intensity than the rest of the urban areas. The large green areas that exist within the EMU campus contribute to this situation. Therefore, there is a mitigating effect on nocturnal LST and SUHI. The statistical analysis reports a relationship between SUHI and LST, PV, LULC, and NDVI. However, it is important to report that the reported SUHI minimization values are lower than those reported in other studies on university campuses (Addas et al., 2020; Cheng et al., 2020; Wibowo et al., 2020). This variation should be attributed to differences in the local climate, geographical location, urban planning of the adjacent cities, and to the extent of the vegetation zones that each campus presents. On the other hand, it is important to take into account the factor of the proximity to the sea. Both the campus of the EMU and the city where they are located are attached to the coastline. For this reason, the UHI effect could present lower intensities since water acts as a moderator of thermal variations being an important factor in the control of ambient temperature (Cuerdo-Vilches et al., 2023; Hidalgo, 2022).

A great diurnal and nocturnal variability of the UHS spaces has been evidenced. It is evident that this circumstance is motivated by the variability of the LST and SUHI already reviewed and that has been evidenced by statistical analysis. During the mornings, the UHS zones have been located mainly in rural areas while during the nights, the UHS zones have been located in urban areas, mainly in compact high-density areas. There are numerous studies (Shahfahad et al., 2021; Sharma et al., 2021) that show identical situations with the UHS identified, validating the results obtained. However, these studies are based on a single image not reporting the variability between night and day. Concerning the EMU Campus area, it should be noted that its distribution and configuration have made it possible not to have daytime UHS and only 1% of its area is affected by night UHS. Exhibiting lower figures than the average values obtained in urban areas contributes to the quality of life of the students who live within the campus and at the same time, indicates that it does not negatively affect the city's climate. Therefore, the climatic conditions of the city are typical of its construction, morphological, and green areas characteristics.

The notable difference between day and night in UTFVI areas has been evident in this study. During the daytime, the predominant classes are 2, 1, and 3, while at night, classes 3 and 4 dominate. Class 1 is primarily situated in rural areas, whereas class 3 is more commonly found in urban areas. This distinction is driven by the spatial variability observed in LST and SUHI values, as discussed previously. In the mornings, LST tends to be higher in rural areas, whereas at night, LST is higher in urban areas due to the characteristics of impermeable construction materials and their high thermal absorption. This phenomenon is corroborated by numerous studies conducted in other cities or urban areas (Guha, 2017; Majumder et al., 2021; Shahfahad et al., 2021), lending support to the results presented in this study.

5 Conclusions

This study analysed the distribution of SUHI, LST, UTFVI, and UHS during July and August 2022 in the city of Famagusta and the EMU Campus. It also studied the relationship between LST and PV, NDVI indices, motivated by the need to identify the spatial variability of the nocturnal and diurnal UHS and UTFVI variables. The goal was to obtain a comprehensive overview that can inform climate change mitigation measures for future university campuses. The results of this study are particularly relevant in light of reports of high temperatures and heat waves in the northern hemisphere during the summer of 2022 and 2023.

Changes in the different LULC coverages motivated by urban growth and development or the construction of new university campuses with large extensions alter the urban climate through the appearance or intensification of the UHI phenomenon. This can greatly alter the quality of life of the people who live in these areas. This is mainly due to the use of waterproof materials with high thermal absorption that, after heating, release heat into the atmosphere and the scarcity of green areas. Our research results on the EMU campus have reported that its morphological configuration with low-rise buildings, with large separation distances and large green areas, greatly minimizes this phenomenon and does not alter the climatic conditions of the city where it is located. In more detail, the structure of urban development

in EMU facilitates the minimization of LST, SUHI, and UHS and improves the quality of the UTFVI index. Therefore, it is suggested that higher education administration in the region use the results of this study as a standard for making future decisions on establishing new universities or modifying older ones. On the other hand, and taking into account that the world-known LCZ classification has been used for the study, our results could be extrapolated to other future campuses that may be carried out in the coming years in different parts of the planet and that have similar characteristics.

Authors' Contributions The research and writing of the document have been carried out equally by both authors.

Funding Funding for open access publishing: Universidad de Granada/CBUA.

Data Availability The research data will be available upon request to the corresponding author.

Code Availability (Software Application or Custom Code) Not applicable.

Declarations

Ethics Approval The authors indicate that all the ethical principles governing the publication of a research article in a journal have been followed.

Conflicts of Interest/Competing Interests (include Appropriate Disclosures) The authors indicate that there are no conflicts of interest.

Consent to Participate The authors agree to participate in the review process and subsequent publication in the event of such an event.

Consent for Publication If the article is accepted, the authors consent to the publication and transfer of the information to the journal.

References

Addas, A., Goldblatt, R., & Rubinyi, S. (2020). Utilizing remotely sensed observations to estimate the urban heat Island effect at a local scale: Case study of a University campus. *Land, 9*(6), 191. https://doi.org/10.3390/LAND9060191

Agam, N., Kustas, W. P., Anderson, M. C., Li, F., & Colaizzi, P. D. (2007). Utility of thermal sharpening over Texas high plains irrigated agricultural fields. *Journal of Geophysical Research Atmospheres, 112*(19), 1–10. https://doi.org/10.1029/2007JD008407

Alcock, I., White, M. P., Lovell, R., Higgins, S. L., Osborne, N. J., Husk, K., & Wheeler, B. W. (2015). What accounts for "England's green and pleasant land"? A panel data analysis of mental health and land cover types in rural England. *Landscape and Urban Planning, 142*, 38–46. https://doi.org/10.1016/j.landurbplan.2015.05.008

Amindin, A., Pouyan, S., Pourghasemi, H. R., Yousefi, S., & Tiefenbacher, J. P. (2021). Spatial and temporal analysis of urban heat island using Landsat satellite images. *Environmental Science and Pollution Research, 28*(30), 41439–41450. https://doi.org/10.3390/rs70810737

An, N., Dou, J., González-Cruz, J. E., Bornstein, R. D., Miao, S., & Li, L. (2020). An observational case study of synergies between an intense heat wave and the urban heat island in Beijing. *Journal of Applied Meteorology and Climatology, 59*(4), 605–620. https://doi.org/10.1175/JAMC-D-19-0125.1

Anjos, M., Targino, A. C., Krecl, P., Oukawa, G. Y., & Braga, R. F. (2020). Analysis of the urban heat island under different synoptic patterns using local climate zones. *Building and Environment, 185*(9), 107268. https://doi.org/10.1016/j.buildenv.2020.107268

Arbuthnott, K. G., & Hajat, S. (2017). The health effects of hotter summers and heat waves in the population of the United Kingdom: A review of the evidence. *Environmental Health: A Global Access Science Source, 16*(1), 1–13. https://doi.org/10.1186/s12940-017-0322-5

Arnfield, A. J. (2003). Two decades of urban climate research: A review of turbulence, exchanges of energy and water, and the urban heat island. *International Journal of Climatology, 23*(1), 1–26. https://doi.org/10.1002/joc.859

Avdan, U., & Jovanovska, G. (2016). Algorithm for automated mapping of land surface temperature using LANDSAT 8 satellite data. *Journal of Sensors*, *2016*. https://doi.org/10.1155/2016/1480307

Belgiu, M., & Stein, A. (2019). Spatiotemporal image fusion in remote sensing. *Remote Sensing, 11*(7), 818. https://doi.org/10.3390/rs11070818

Blessy, A., John Paul, J., & Gautam, S. (2023). IoT-Based Air Quality Monitoring in Hair Salons: Screening of Hazardous Air Pollutants Based on Personal Exposure and Health Risk Assessment. *Water, Air, and Soil Pollution, 234*, 336. https://doi.org/10.1007/s11270-023-06350-4

Brousse, O., Georganos, S., Demuzere, M., Vanhuysse, S., Wouters, H., Wolff, E., Linard, C., van Lipzig, N. P. M., & Dujardin, S. (2019). Using Local Climate Zones in Sub-Saharan Africa to tackle urban health issues. *Urban Climate, 27*(12), 227–242. https://doi.org/10.1016/j.uclim.2018.12.004

Chen, Y., Li, X., Zheng, Y., Guan, Y., & Liu, X. (2011). Estimating the relationship between urban forms and energy consumption: A case study in the Pearl River Delta, 2005–2008. *Landscape and Urban Planning, 102*(1), 33–42. https://doi.org/10.1016/j.landurbplan.2011.03.007

Cheng, D., Gao, C., Shao, T., & Iqbal, J. (2020). A landscape study of sichuan university (Wangjiang campus) from the perspective of campus tourism. *Land, 9*(12), 1–21. https://doi.org/10.3390/land9120499

Chun, B., & Guldmann, J. M. (2014). Spatial statistical analysis and simulation of the urban heat island in high-density central cities. *Landscape and Urban Planning, 125*, 76–88. https://doi.org/10.1016/j.landurbplan.2014.01.016

Cuerdo-Vilches, T., Díaz, J., López-Bueno, J. A., Luna, M. Y., Navas, M. A., Mirón, I. J., & Linares, C. (2023). Impact of urban heat islands on morbidity and mortality in heat waves: Observational time series analysis of Spain's five cities. *Science of the Total Environment, 890*, 164412. https://doi.org/10.1016/j.scitotenv.2023.164412

Das, M., & Das, A. (2020). Assessing the relationship between local climatic zones (LCZs) and land surface temperature (LST) – A case study of Sriniketan-Santiniketan Planning Area (SSPA), West Bengal. *India. Urban Climate, 32*, 100591. https://doi.org/10.1016/j.uclim.2020.100591

Diallo-Dudek, J., Lacaze, B., & Comby, J. (2015). Land surface temperature in the urban area of Lyon metropolis: A comparative study of remote sensing data and MesoNH model simulation. *2015 Joint Urban Remote Sensing Event*. *JURSE, 2015*, 2–5. https://doi.org/10.1109/JURSE.2015.7120528

Du, J., Xiang, X., Zhao, B., & Zhou, H. (2020). Impact of urban expansion on land surface temperature in Fuzhou, China using Landsat imagery. *Sustainable Cities and Society, 61*(6), 102346. https://doi.org/10.1016/j.scs.2020.102346

Dwivedi, A., & Mohan, B. K. (2018). Impact of green roof on micro climate to reduce Urban Heat Island. *Remote Sensing Applications: Society and Environment, 10*, 56–69. https://doi.org/10.1016/j.rsase.2018.01.003

Equere, V., Mirzaei, P. A., & Riffat, S. (2020). Definition of a new morphological parameter to improve prediction of urban heat island. *Sustainable Cities and Society, 56*(11), 102021. https://doi.org/10.1016/j.scs.2020.102021

Fang, L., & Tian, C. (2020). Construction land quotas as a tool for managing urban expansion. *Landscape and Urban Planning, 195*, 103727. https://doi.org/10.1016/j.landurbplan.2019.103727

García, D. H., & Díaz, J. A. (2023). Space–time analysis of the earth's surface temperature, surface urban heat island and urban hotspot: Relationships with variation of the thermal field in Andalusia (Spain). *Urban Ecosystems, 26*, 525–547. https://doi.org/10.1007/s11252-022-01321-9

García-Santos, V., Cuxart, J., Martínez-Villagrasa, D., Jiménez, M. A., & Simó, G. (2018). Comparison of three methods for estimating land surface temperature from Landsat 8-TIRS Sensor data. *Remote Sensing, 10*(9), 1–13. https://doi.org/10.3390/rs10091450

Gaur, A., Eichenbaum, M. K., & Simonovic, S. P. (2018). Analysis and modelling of surface Urban Heat Island in 20 Canadian cities under climate and land-cover change. *Journal of Environmental Management, 206*, 145–157. https://doi.org/10.1016/j.jenvman.2017.10.002

Guha, S. (2017). Dynamic analysis and ecological evaluation of urban heat islands in Raipur city. *India. Journal of Applied Remote Sensing, 11*(03), 1. https://doi.org/10.1117/1.jrs.11.036020

Guha, S., Govil, H., Dey, A., & Gill, N. (2018). Analytical study of land surface temperature with NDVI and NDBI using Landsat 8 OLI and TIRS data in Florence and Naples city. *Italy. European Journal of Remote Sensing, 51*(1), 667–678. https://doi.org/10.1080/22797254.2018.1474494

Hidalgo, D. (2022). Analysis of Urban Heat Island and Heat Waves Using Sentinel-3 Images: A Study of Andalusian Cities in Spain. *Earth Systems and Environment, 6*, 199–219. https://doi.org/10.1007/s41748-021-00268-9

Hidalgo, D. (2023). Spatio-temporal analysis of the urban green infrastructure of the city of Granada (Spain) as a heat mitigation measure using high-resolution images Sentinel 3. *Urban Forestry & Urban Greening, 87*, 128061. https://doi.org/10.1016/j.ufug.2023.128061

Hidalgo García, D., & Arco Díaz, J. (2021). Modeling of the Urban Heat Island on local climatic zones of a city using Sentinel 3 images: Urban determining factors. *Urban Climate, 37*, 100840. https://doi.org/10.1016/j.uclim.2021.100840

Hidalgo García, D., & Arco-Díaz, J. (2022). Modeling the Surface Urban Heat Island (SUHI) to study of its relationship with variations in the thermal field and with the indices of land use in the metropolitan area of Granada (Spain). *Sustainable Cities and Society, 87*, 104167. https://doi.org/10.1016/j.scs.2022.104166

Hu, Y., Dai, Z., & Guldmann, J. M. (2020). Modeling the impact of 2D/3D urban indicators on the urban heat island over different seasons: A boosted regression tree approach. *Journal of Environmental Management, 266*(11), 110424. https://doi.org/10.1016/j.jenvman.2020.110424

Huryna, H., Cohen, Y., Karnieli, A., Panov, N., Kustas, W. P., & Agam, N. (2019). Evaluation of TsHARP utility for thermal sharpening of Sentinel-3 satellite images using Sentinel-2 visual imagery. *Remote Sensing, 11*(19), 2304. https://doi.org/10.3390/rs11192304

Kafy, A. A., Faisal, A. A., Rahman, M. S., Islam, M., Al Rakib, A., Islam, M. A., Khan, M. H. H., Sikdar, M. S., Sarker, M. H. S., Mawa, J., & Sattar, G. S. (2021). Prediction of seasonal urban thermal field variance index using machine learning algorithms in Cumilla, Bangladesh. *Sustainable Cities and Society, 64*, 102542. https://doi.org/10.1016/j.scs.2020.102542

Keeratikasikorn, C., & Bonafoni, S. (2018). Urban heat island analysis over the land use zoning plan of Bangkok by means of Landsat 8 imagery. *Remote Sensing, 10*(3), 440. https://doi.org/10.3390/rs10030440

Lemus-Canovas, M., Martin-Vide, J., Moreno-Garcia, M. C., & Lopez-Bustins, J. A. (2020). Estimating Barcelona's metropolitan daytime hot and cold poles using Landsat-8

Land Surface Temperature. *Science of the Total Environment, 699*, 134307. https://doi.org/10.1016/j.scitotenv.2019.134307

Lin, W., Yu, T., Chang, X., Wu, W., & Zhang, Y. (2015). Calculating cooling extents of green parks using remote sensing: Method and test. *Landscape and Urban Planning, 134*, 66–75. https://doi.org/10.1016/j.landurbplan.2014.10.012

Liu, L., & Zhang, Y. (2011). Urban heat island analysis using the landsat TM data and ASTER Data: A case study in Hong Kong. *Remote Sensing, 3*(7), 1535–1552. https://doi.org/10.3390/rs3071535

Macintyre, H. L., Heaviside, C., Taylor, J., Picetti, R., Symonds, P., Cai, X. M., & Vardoulakis, S. (2018). Assessing urban population vulnerability and environmental risks across an urban area during heatwaves – Implications for health protection. *Science of the Total Environment, 610–611*, 678–690. https://doi.org/10.1016/j.scitotenv.2017.08.062

Majumder, A., Setia, R., Kingra, P. K., Sembhi, H., Singh, S. P., & Pateriya, B. (2021). Estimation of land surface temperature using different retrieval methods for studying the spatiotemporal variations of surface urban heat and cold islands in Indian Punjab. *Environment, Development and Sustainability, 23*(11), 15921–15942. https://doi.org/10.1007/s10668-021-01321-3

Nicholson, S. E., & Farrar, T. J. (1994). The influence of soil type on the relationships between NDVI, rainfall, and soil moisture in semiarid Botswana. I. NDVI response to rainfall. *Remote Sensing of Environment, 50*(2), 107–120. https://doi.org/10.1016/0034-4257(94)90038-8

Oke, T. R. (1987). *Boundary layer climates* (Routledge).

Otukei, J. R., & Blaschke, T. (2010). Land cover change assessment using decision trees, support vector machines and maximum likelihood classification algorithms. *International Journal of Applied Earth Observation and Geoinformation, 12*(SUPPL. 1), S27. https://doi.org/10.1016/j.jag.2009.11.002

Qiu, G. Y., Zou, Z., Li, X., Li, H., Guo, Q., Yan, C., & Tan, S. (2017). Experimental studies on the effects of green space and evapotranspiration on urban heat island in a subtropical megacity in China. *Habitat International, 68*, 30–42. https://doi.org/10.1016/j.habitatint.2017.07.009

Qiu, T., Song, C., Clark, J. S., Seyednasrollah, B., Rathnayaka, N., & Li, J. (2020). Understanding the continuous phenological development at daily time step with a Bayesian hierarchical space-time model: Impacts of climate change and extreme weather events. *Remote Sensing of Environment, 247*(11), 111956. https://doi.org/10.1016/j.rse.2020.111956

Rajeshwari, A. (2014). Estimation of land surface temperature of dindigul district using landsat 8 data. *International Journal of Research in Engineering and Technology, 03*(05), 122–126. https://doi.org/10.15623/ijret.2014.0305025

Rezapouraghdam, H., & Vahedi, S. (2024). Exploring educational tourists' perceptions of climate change on a small Mediterranean island: A qualitative analysis. *Worldwide Hospitality and Tourism Themes*. https://doi.org/10.1108/WHATT-12-2023-0144

Rezapouraghdam, H., Alipour, H., Kilic, H., & Akhshik, A. (2022a). Education for sustainable tourism development: An exploratory study of key learning factors. *Worldwide Hospitality and Tourism Themes, 14*(4), 384–392.

Rezapouraghdam, H., Karatepe, O., & Enea, C. (2022b). Sustainable recovery for people and the planet through spirituality-induced connectedness in the hospitality and tourism industry. *Journal of Hospitality and Tourism Insights, 6*(5), 1776–1995. https://doi.org/10.1108/JHTI-03-2022-0103

Saaroni, H., Amorim, J. H., Hiemstra, J. A., & Pearlmutter, D. (2018). Urban Green Infrastructure as a tool for urban heat mitigation: Survey of research methodologies and findings across different climatic regions. *Urban Climate, 24*, 94–110. https://doi.org/10.1016/j.uclim.2018.02.001

Safarrad, T., Ghadami, M., Dittmann, A., & Pazhuhan, M. (2021). Tourism effect on the spatiotemporal pattern of land surface temperature (Lst): Babolsar and fereydonkenar cities (cases study in Iran). *Land, 10*(9), 945. https://doi.org/10.3390/land10090945

Santamouris, M. (2020). Recent progress on urban overheating and heat island research. Integrated assessment of the energy, environmental, vulnerability and health impact. Synergies with the global climate change. *Energy and Buildings, 207*, 109482. https://doi.org/10.1016/j.enbuild.2019.109482

Scolozzi, R., & Geneletti, D. (2012). A multi-scale qualitative approach to assess the impact of urbanization on natural habitats and their connectivity. *Environmental Impact Assessment Review, 36*, 9–22. https://doi.org/10.1016/j.eiar.2012.03.001

Sekertekin, A., & Bonafoni, S. (2020). Land surface temperature retrieval from Landsat 5, 7, and 8 over rural areas: Assessment of different retrieval algorithms and emissivity models and toolbox implementation. *Remote Sensing, 12*(2), 294. https://doi.org/10.3390/rs12020294

Shahfahad, Talukdar, S., Rihan, M., Hang, H. T., Bhaskaran, S., & Rahman, A. (2021). Modelling urban heat island (UHI) and thermal field variation and their relationship with land use indices over Delhi and Mumbai metro cities. *Environment, Development and Sustainability, 34*(6), 3762. https://doi.org/10.1007/s10668-021-01587-7

Sharma, R., Pradhan, L., Kumari, M., & Bhattacharya, P. (2021). Assessing urban heat islands and thermal comfort in Noida City using geospatial technology. *Urban Climate, 35*, 100751. https://doi.org/10.1016/j.uclim.2020.100751

Sharma, A., Pandher, J. S., & Prakash, G. (2022). Consumer confusion and decision postponement in the online tourism domain: the moderating role of self-efficacy. *Journal of Hospitality and Tourism Insights*. https://doi.org/10.1108/JHTI-03-2O22-0096

Song, J., Lin, T., Li, X., & Prishchepov, A. V. (2018). Mapping urban functional zones by integrating very high spatial resolution remote sensing imagery and points of interest: A case study of Xiamen, China. *Remote Sensing, 10*(11), 1737. https://doi.org/10.3390/rs10111737

Song, J., Chen, W., Zhang, J., Huang, K., Hou, B., & Prishchepov, A. V. (2020). Effects of building density on land surface temperature in China: Spatial patterns and

determinants. *Landscape and Urban Planning, 198*, 103794. https://doi.org/10.1016/j.landurbplan.2020.103794

Stewart, I. D. (2011). A systematic review and scientific critique of methodology in modern urban heat island literature. *International Journal of Climatology, 31*(2), 200–217. https://doi.org/10.1002/joc.2141

Stewart, I., & Oke, T. (2009). Classifying urban climate field sites by "local climate zones": the case of nagano, Japan. *The Seventh International Conference on Urban Climate*, *July*, 1–5.

Stewart, I. D., & Oke, T. R. (2012). Local climate zones for urban temperature studies. *Bulletin of the American Meteorological Society, 93*(12), 1879–1900. https://doi.org/10.1175/BAMS-D-11-00019.1

Suhail, M., Khan, M. S., & Faridi, R. A. (2019). Assessment of urban heat islands effect and land surface temperature of noida, india by using landsat satellite data. *Mapan - Journal of Metrology Society of India, 34*(4), 431–441. https://doi.org/10.1007/s12647-019-00309-9

Tepanosyan, G., Muradyan, V., Hovsepyan, A., Pinigin, G., Medvedev, A., & Asmaryan, S. (2021). Studying spatial-temporal changes and relationship of land cover and surface Urban Heat Island derived through remote sensing in Yerevan Armenia. *Building and Environment, 187*, 107390. https://doi.org/10.1016/j.buildenv.2020.107390

UNO. (2018). *68% of the world population projected to live in urban areas by 2050, says UN.* https://www.un.org/development/desa/en/news/population/2018-revision-of-world-urbanization-prospects.html. Accessed 05/08/2023.

van Hove, L. W. A., Jacobs, C. M. J., Heusinkveld, B. G., Elbers, J. A., Van Driel, B. L., & Holtslag, A. A. M. (2015). Temporal and spatial variability of urban heat island and thermal comfort within the Rotterdam agglomeration. *Building and Environment, 83*, 91–103. https://doi.org/10.1016/j.buildenv.2014.08.029

Wang, T., Shi, J., Ma, Y., Husi, L., Comyn-Platt, E., Ji, D., Zhao, T., & Xiong, C. (2019). Recovering land surface temperature under cloudy skies considering the solar-cloud-satellite geometry: application to modis and landsat-8 data. *Journal of Geophysical Research: Atmospheres, 124*(6), 3401–3416. https://doi.org/10.1029/2018JD028976

Wibowo, A., Yusoff, M. M., Hamzah, T. A. A., Binti, T., & Shidiq, I. P. A. (2020). Urban heat hazard threat on University Campus (University of Indonesia and University of Malaya). *International Journal of GEOMATE, 19*(76), 141–148. https://doi.org/10.21660/2020.76.95107

Wu, C., Li, J., Wang, C., Song, C., Chen, Y., Finka, M., & La Rosa, D. (2019). Understanding the relationship between urban blue infrastructure and land surface temperature. *Science of the Total Environment*, 694. https://doi.org/10.1016/j.scitotenv.2019.133742

Xu, D., Kang, X., Qiu, D., Zhuang, D., & Pan, J. (2009). Quantitative assessment of desertification using Landsat data on a regional scale - a case study in the Ordos Plateau. *China. Sensors, 9*(3), 1738–1753. https://doi.org/10.3390/s90301738

Yang, C., Wang, R., Zhang, S., Ji, C., & Fu, X. (2019). Characterizing the hourly variation of urban heat islands in a snowy climate city during summer. *International Journal of Environmental Research and Public Health, 16*(14). https://doi.org/10.3390/ijerph16142467

Yang, C., Yan, F., & Zhang, S. (2020a). Comparison of land surface and air temperatures for quantifying summer and winter urban heat island in a snow climate city. *Journal of Environmental Management, 265*, 110563. https://doi.org/10.1016/j.jenvman.2020.110563

Yang, J., Zhou, J., Göttsche, F.-M., Long, Z., Ma, J., & Luo, R. (2020b). Investigation and validation of algorithms for estimating land surface temperature from Sentinel-3 SLSTR data. *International Journal of Applied Earth Observation and Geoinformation, 91*, 102136. https://doi.org/10.1016/j.jag.2020.102136

Yin, Z., Liu, Z., Liu, X., Zheng, W., & Yin, L. (2023). Urban heat islands and their effects on thermal confort in the US: New York and Jersey. *Ecological Indicators, 154*, 110765. https://doi.org/10.1016/j.ecolind.2023.110765

Yu, X., Guo, X., & Wu, Z. (2014). Land surface temperature retrieval from landsat 8 TIRS comparison between radiative transfer equation-based method, split window algorithm and single channel method. *Remote Sensing, 6*(10), 9829–9852. https://doi.org/10.3390/rs6109829

Zhang, S., Bai, X., Zhao, C., Tan, Q., Luo, G., & Wang, J. (2021). Global CO_2 consumption by silicate rock chemical weathering: Its past and future. *Earth's Future, 9*, e2020EF001938. https://doi.org/10.1029/2020EF001938

Zhao, R., Huang, X., Xue, J., & Guan, X. (2023). A practical simulation of carbon sink calculation for urban buildings: A case study of Zhengzhou in China. *Sustainable Cities and Society, 99*, 104980. https://doi.org/10.1016/j.scs.2023.104980

Zhengtong, Y., Zhixin, L., Xuan, L., Wenfeng, Z., & Lirong, Y. (2023). Urban heat islands and their effects on thermal comfort in the US: New York and New Jersey. *Ecological Indicators, 154*, 110765. https://doi.org/10.1016/j.ecolind.2023.110765

Zhou, X., Wang, P., Tansey, K., Zhang, S., Li, H., & Tian, H. (2020). Reconstruction of time series leaf area index for improving wheat yield estimates at field scales by fusion of Sentinel-2, -3 and MODIS imagery. *Computers and Electronics in Agriculture, 177*(17), 105692. https://doi.org/10.1016/j.compag.2020.105692